HIGHLY OXIDIZED COMPOUNDS FROM HETEROGENEOUS OXIDATION OF ISOPRENE EPOXYDIOL (IEPOX)-DERIVED SECONDARY ORGANIC AEROSOL (SOA) IDENTIFIED USING HYDROPHILIC INTERACTION LIQUID CHROMATOGRAPHY INTERFACED TO ELECTROSPRAY IONIZATION HIGH-RESOLUTION QUADRUPOLE TIME-OF-FLIGHT MASS SEPCTROMETRY (HILIC/ESI-HR-QTOFMS)

Caz Armstrong Nichols

A thesis submitted to the faculty at the University of North Carolina at Chapel Hill in partial fulfillment of the requirements for the degree of Master of Science in the Department of Environmental Science and Engineering in the Gillings School of Global Public Health.

Chapel Hill
2020

Approved by:

Jason D. Surratt

Barbara J. Turpin

Avram Gold

Havala O. T. Pye

ABSTRACT

Caz Armstrong Nichols: Highly Oxidized Compounds from Heterogeneous Oxidation of Isoprene Epoxydiol (IEPOX)-Derived Secondary Organic Aerosol (SOA) Identified using Hydrophilic Interaction Liquid Chromatography interfaced to Electrospray Ionization High-Resolution Quadrupole Time-of-Flight Mass Spectrometry (HILIC/ESI-HR-QTOFMS)
(Under the direction of Jason D. Surratt)

Atmospheric fine particulate matter ($PM_{2.5}$) is critical to climate, air quality, and human health. Acid-driven multiphase chemistry of isoprene-derived epoxydiols (IEPOX) substantially contributes to secondary organic aerosol (SOA) formation. However, atmospheric chemical sinks of freshly-generated IEPOX-derived SOA remain unclear, and thus, are not considered in atmospheric chemistry models. We systematically examined the role of heterogeneous oxidation of authentic IEPOX-derived SOA particles by gas-phase hydroxyl radical (OH) as one potential atmospheric sink. Chemical changes in smog chamber-generated IEPOX-derived SOA were assessed after 1 and 4 hours of gas-phase OH exposure by collection on Teflon filters and using hydrophilic interaction liquid chromatography interfaced to electrospray ionization high-resolution quadrupole time-of-flight mass spectrometry (HILIC/ESI-HR-QTOFMS). Tentative structures and formation mechanisms are proposed here for previously measured ambient $PM_{2.5}$ constituents with uncertain chemical sources; specifically, they form from oxidative aging of the most abundant, freshly-generated IEPOX-derived SOA constituents, including 2-methyltetrols, 2-methyltetrol sulfates and the corresponding dimers.

ACKNOWLEDGEMENTS

I would like to thank the members of my committee, including my advisor - Jason D. Surratt, PhD, and my committee members - Barbara Turpin, PhD, Avram Gold, PhD, and Havala O. T. Pye, PhD. Without your support and guidance, this work would not have come to fruition. I would also like to thank the members of the Surratt and Turpin laboratories for your mentorship, encouragement, and advice. Finally, I would like to thank the Department of Environmental Science and Engineering and the National Institute for Occupational Safety and Health (grant no. T42-OH008673) for generously providing funding to pursue my graduate degree. HILIC/ESI-HR-QTOFMS work was performed in the UNC Biomarker Mass Spectrometry Facility, which is supported by the National Institute of Environmental Health Sciences (grant no. P30ES010126). This work is funded by the National Science Foundation (NSF) (grant no. AGS-1703535).

TABLE OF CONTENTS

LIST OF SCHEMES

LIST OF TABLES

LIST OF FIGURES

LIST OF ABBREVIATIONS

2-MTs	2-methyltetrols, $C_5H_{12}O_4$
2-MTSs	2-methyltetrol sulfates, $C_5H_{12}O_7S$
EIC	Extracted ion chromatogram
HILIC/ESI-HR-QTOFMS	Hydrophilic interaction liquid chromatography interfaced to electrospray ionization high-resolution quadrupole time-of-flight mass spectrometry
IEPOX	Isoprene epoxydiols, $C_5H_{10}O_3$
NO	Nitric oxide
$^{\bullet}OH$	hydroxyl radical
OS	Organosulfate
OS_C	Oxidation state of carbon
PILS	Particle Into Liquid Sampler
$PM_{2.5}$	Particulate matter fraction ≤ 2.5 μm in aerodynamic diameter
RNS	Reactive nitrogen species, a biomarker for inflammation
ROS	Reactive oxygen species, a biomarker for inflammation
RPLC	Reverse-phase liquid chromatography
SOA	Secondary organic aerosol
$Sulf_{inorg}$	Inorganic sulfate aerosol
TIC	Total ion chromatogram
VOC	Volatile organic compound

CHAPTER 1: INTRODUCTION

Secondary organic aerosol (SOA) derived from the atmospheric oxidation of volatile organic compounds (VOCs) is estimated to comprise 70-90% of the organic mass fraction of ambient fine particulate matter with aerodynamic diameters ≤ 2.5 μm ($PM_{2.5}$).[1] Isoprene has the highest emission flux of any non-methane VOC,[2] making it a likely significant SOA precursor for a large fraction of atmospheric $PM_{2.5}$ mass.[3-6] Under low-nitric oxide (NO) conditions, isoprene-derived SOA primarily forms through the acid-catalyzed multiphase (reactive uptake) chemistry of isoprene epoxydiols (IEPOX),[7-10] which are the most abundant second-generation gas-phase oxidation products from isoprene under these conditions.[8,11] Reactive uptake kinetics of IEPOX depends strongly on aerosol acidity,[10,12-14] liquid water content,[12,15] morphology,[12,14,16] and inorganic sulfate ($Sulf_{inorg}$) concentration.[16] Recently, Riva et al.[16] demonstrated that at high IEPOX/$Sulf_{inorg}$ ratios the acid-catalyzed reactive uptake of IEPOX to $Sulf_{inorg}$ aerosol particles converts up to 90% of particulate $Sulf_{inorg}$ to organosulfates (OSs), which alters the aerosol physiochemical properties (viscosity, volatility, phase state, morphology, and acidity) of $Sulf_{inorg}$ aerosol.[17] Field studies have found that ~75% or more of fine particulate OSs may be derived from isoprene,[18] where the most abundant atmospheric OSs are the 2-methyltetrol sulfate diastereomers (2-MTSs), which are known to be derived from reactive uptake of IEPOX. Reactive uptake of IEPOX to acidic $Sulf_{inorg}$ aerosol particles efficiently produces SOA through low-volatility OS formation;[16,17.19-21] the addition of functional groups such as OH and OSO_3H lowers the volatility of parent VOCs by orders of magnitude.[22-24]

As a result of their low volatility, OSs, such as 2-MTSs, are thought to have long atmospheric lifetimes,[25,26] substantially contributing to $PM_{2.5}$ mass in the lower and upper troposphere as well as likely playing a role in cloud formation.[27] 2-MTSs have been measured to contribute up to 13% of the total organic carbon in $PM_{2.5}$ collected from ground sites in downtown Atlanta, GA,[28] and up to 10% of OA mass at sites in Look Rock, TN[26] and Manaus, Brazil,[29] making 2-MTSs among the single most abundant compounds detected in $PM_{2.5}$ collected from isoprene-rich regions. Notably, 2-MTSs and other isoprene-derived OSs have also been measured in free (upper) tropospheric submicron particles,[25,30,31] cloud water samples[32,33] and certain precipitation types such as hailstones and rain.[34] Although IEPOX-derived OSs, including 2-MTSs, have been measured in various atmospheric media, it remains unclear whether these compounds have atmospheric chemical sinks such as heterogeneous oxidation of aerosols by hydroxyl radical ($^{\bullet}OH$) or by cloud water oxidation chemistry. Because a large fraction of $PM_{2.5}$ may be derived from the acid-catalyzed multiphase chemistry of IEPOX, particular chemical sinks, especially heterogeneous $^{\bullet}OH$ oxidation of existing $PM_{2.5}$ containing IEPOX-derived SOA, are of great interest to investigate in order to determine the atmospheric lifetime of these aerosol constituents. Not all atmospheric models include IEPOX-derived SOA formation and its resultant OSs; those that do assume IEPOX-derived SOA and its OSs remain unreactive toward heterogeneous oxidation by gas-phase $^{\bullet}OH$.[35,36]

Although investigation is still in its infancy, the health effects of isoprene-derived SOA may be worth considering in air pollution mitigation strategies, but more work is needed.[37] Prior work has shown that isoprene-derived SOA alters expression of genes that regulate antioxidant defenses in human lung cell models, suggesting that isoprene-derived SOA leads to an increase in cellular oxidant burden.[37] Isoprene-derived SOA, including freshly-generated IEPOX-derived

SOA, has been shown to cause similar (in some cases greater) oxidative stress compared to fresh and aged diesel-derived PM.[38] Furthermore, average carbon oxidation state (OS_C) has been shown to correlate with higher reactive oxygen and nitrogen species (ROS/RNS) responses, which are measures of cellular inflammation.[39] Notably, work by Rattanavaraha et al.[40] demonstrated that oxidative aging with gas-phase •OH enhanced the oxidative potential of freshly-generated diesel-derived PM. Since most prior studies have examined the chemical composition and toxicological properties of freshly-generated IEPOX-derived SOA,[10,15,41] it is warranted to investigate how the chemical composition of IEPOX-derived SOA particles changes with exposure to •OH. The key question is whether IEPOX-derived SOA particles heterogeneously aged by •OH have higher average OS_C values due to the presence of more functionalized SOA constituents, and thus, potentially contribute to adverse health effects associated with $PM_{2.5}$ exposures in isoprene-rich regions. Further research in this area is needed, especially in first examining the chemical changes of particles due to oxidative aging.

Many studies have investigated the oxidation of isoprene, IEPOX, and other intermediates leading to SOA, during both laboratory studies[11,22,42-47] and field studies.[18,48-52] However, most have been confined to proposing empirical formulas for some of the many oxidation products due to the lack of authentic standards and/or tandem mass spectrometry data.[22,46,47] Currently, IEPOX-derived compounds appear to account for a large portion of isoprene SOA in ambient aerosol;[5,53] however, many isoprene-related OSs and organic acids lack known mechanisms of formation, preventing their inclusion in atmospheric chemistry models. Additionally, many IEPOX SOA experiments have been conducted in the dark without the presence of •OH,[10,12-16,54] a key atmospheric oxidant during the daytime, particularly for SOA formation.[55-57] Only three studies have conducted significant work on heterogeneous •OH oxidation of IEPOX-derived SOA,

including one using ambient $PM_{2.5}$ containing IEPOX-derived SOA collected during a field study,[58] one using aerosol containing authentic 3-methyltetrol sulfate, which is a minor IEPOX-derived OS product, during a controlled laboratory study,[46] and one using aerosol containing authentic 2-MTSs during a controlled laboratory study.[59] All three studies were conducted in an oxidation flow reactor with a residence time under five minutes and with elevated •OH levels (i.e., $\sim 10^{11\text{-}13}$ molecules cm^{-3}), orders of magnitude more than is common in the atmosphere (i.e., $\sim 10^{6}$ molecules cm^{-3}).[60] These studies did not aim to chemically characterize new SOA constituents at the molecular level that would result from heterogeneous •OH oxidation of the full IEPOX-derived SOA mixture; however, our recent heterogeneous •OH oxidation study with authentic 2-MTS aerosols demonstrated that multifunctional OSs could be produced at atmospherically-relevant time scales of oxidation (~16 days, assuming an average daytime OH concentration of 1.5×10^{6} molecules cm^{-3}),[59] and that these newly identified heterogeneous oxidation-derived OS products have been previously measured in ground level and free tropospheric $PM_{2.5}$, as well as in cloud water and hailstones.[29-34,59]

IEPOX reactive uptake results in phase separation or salting-out of organics, such as the 2-MTSs and related OSs as well as the 2-methyltetrols (2-MTs), forming a viscous organic shell around an aqueous inorganic core.[16,17,61-66] This impedes further uptake of IEPOX into the aerosol phase due to lack of mobility within the particle.[14] This means that IEPOX-derived OSs (and possibly 2-MTs) become sequestered on the outside of a particle, increasing the probability of exposure to gas-phase oxidants like •OH. Thus, after a period of reactive uptake, particles should begin to undergo heterogeneous •OH oxidation if these surface-bound SOA constituents are sufficiently reactive with •OH. The role of heterogeneous •OH oxidation of full IEPOX-derived SOA mixture and its related OSs remains uncertain, especially at longer reaction time scales

(hours) and at lower •OH concentrations than past studies have considered.

This study systematically examined the heterogeneous •OH oxidation of freshly-generated IEPOX-derived SOA in a smog chamber at atmospherically-relevant time scales and •OH concentrations with the aim of proposing structures and reaction pathways for the most abundant IEPOX-derived SOA constituents present in atmospheric aerosol. Heterogeneous •OH oxidation of IEPOX-derived SOA particles is examined through systematic smog chamber studies conducted in the dark and in the presence of •OH at ~50% relative humidity (RH). Non-targeted chemical analyses of fresh versus heterogeneously •OH-aged IEPOX-derived SOA are conducted using hydrophilic interaction liquid chromatography interfaced with electrospray ionization coupled with high-resolution quadrupole time-of-flight mass spectrometry (HILIC/ESI-HR-QTOFMS). HILIC is an alternative and complementary method to reverse-phase liquid chromatography (RPLC). HILIC elution order is similar to normal phase LC, but better separation of highly polar compounds is achieved by column packing designed to be coated by a layer of water.[28] Cui et al.[29] showed that HILIC is more suited than RPLC for highly oxidized and OS-containing isoprene-derived SOA constituents by achieving separation. Heterogeneously •OH-aged IEPOX-derived SOA particles generated during chamber experiments are compared with archived $PM_{2.5}$ samples collected from the Southeastern U.S., the Amazon rainforest, and Galápagos Islands in order to determine if this potential sink for IEPOX-derived SOA is relevant to the atmosphere.

CHAPTER 2: EXPERIMENTAL METHODS

Chamber Experiments. Experiments were conducted in a 10-m^3 indoor smog chamber facility located at the University of North Carolina at Chapel Hill (UNC). Prior to the start of each experiment the smog chamber was flushed with zero air for ~12 h so that the background aerosol volume concentration was <0.1 μm^3 cm^{-3}, as measured by a scanning electrical mobility spectrometer (SEMS) consisting of a differential mobility analyzer (DMA, BMI Inc., model 2002) coupled to a mixing condensation particle counter (MCPC, BMI Inc., model 1710). Background ozone (O_3) concentrations were <5 ppb before the start of each experiment. O_3 was monitored every 10 s by an O_3 analyzer (2B Technologies, model 202). The chamber was humidified to 45-53% RH at 21.5±0.5°C prior to experiments. RH and temperature inside the chamber were measured by a dewpoint meter (Omega Engineering Inc.) recording every 5 s. All experiments summarized in Table 1 were conducted in the absence of UV light sources, and background visible light was minimized.

Heterogeneous $^{\bullet}OH$ oxidation of IEPOX-derived SOA began with the atomization of 90 ± 10 μm^3 cm^{-3} ammonium bisulfate (NH_4HSO_4) seed aerosols using a custom-built atomizer with aqueous solution of 0.06 M NH_4HSO_4 (solution pH=1.7 as measured by a pH probe, Atlas Scientific) which was allowed to become well-mixed in the chamber for 30 min after injection. 15 mg of authentic *trans*-β-IEPOX, which is the predominant IEPOX isomer in the atmosphere,[4,67] was dissolved in ethyl acetate and injected into the chamber by flowing heated nitrogen (67 °C) at 5 L min^{-1} through a glass manifold until aerosol volume growth due to freshly-generated IEPOX-

derived SOA formation ceased, typically after ~1 h of gas-phase IEPOX injection. *Trans*-β-IEPOX was synthesized in-house following published procedures.[68] IEPOX injection efficiencies ranged between 0.5 and 0.9 (see Table 1), as determined by weighing the glass manifold before and after IEPOX injection using an analytical balance (Mettler Toledo Model MS205DU). •OH was created by the reaction of 2 ppm O_3 (injected for ~ 45 s and stopped) with tetramethylethylene (TME, at 280 mL min^{-1} with 5 L min^{-1} sheath flow),[69] where TME was continuously injected for either 1 or 4 h to sustain oxidative aging of freshly-generated IEPOX-derived SOA particles. Immediately before and after the 1- or 4-h oxidative aging by •OH, SOA particles were collected on Teflon filters (0.2-μm pore size, PALL Corp.) for one hour at ~12 L min^{-1}. Some •OH may have been collected with the post-oxidation filter, meaning that potentially SOA could continue to react after collection. However, control experiments using a carbon denuder did not yield significantly different results.

In select experiments (experiments #9 and 10, Table 1), authentic 2-MTS aerosol particles were heterogeneously oxidized by •OH in the dark. 2-MTSs were synthesized in-house as 2-MTS ammonium salts following published procedures.[29] Purity was determined to be ~86% (major impurities identified by HILIC/ESI-HR-QTOFMS analysis were $C_3H_6O_5S$, $C_4H_8O_6S$, and CH_4O_4S). 100 ± 10 μm^3 cm^{-3} of 2-MTS seed aerosols was injected into the chamber using a custom-built atomizer with an aqueous solution of 4.6 mM 2-MTSs and allowed to mix for 30 min. Filter collection and •OH generation procedures were exactly the same as described above for IEPOX-derived SOA.

Control experiments were conducted with no TME injected, and the IEPOX-derived SOA aged for 4 h with only O_3, with which it was not anticipated to react. Recent work from our lab demonstrated that 2-MTS aerosols did not chemically change upon UV-only or O_3-only

exposures.[59] O_3 concentration was directly measured by an O_3 monitor, and average •OH concentration was estimated using a model based on the work of Lambe et al.[69] Because the model does not consider all sinks for OH, this represents an upper bound estimate.

Table 1. Experimental conditions for the heterogeneous •OH oxidation of freshly-generated IEPOX-derived SOA or authentic 2-MTS particles.

Expt #	Initial Aerosol Type	IEPOX Injection Efficiency	Pre-aging SOA Volume Concentration (μm^3 cm^{-3})	Oxidant Type	[Oxidant] (molecule cm^{-3})	RH (%)	Oxidative Aging Time (h)	O_3 Consumed (ppb)
1	IEPOX-SOA	0.85	240	OH	$2.7x10^8$	50	1	437
2	IEPOX-SOA	0.36	145	OH	$2.7 x10^8$	51	1	353
3	IEPOX-SOA	0.45	175	OH	$2.7 x10^8$	52	1	371
4	IEPOX-SOA	0.72	225	OH	$2.9 x10^8$	51	4	1617
5	IEPOX-SOA	0.73	250	OH	$2.9 x10^8$	53	4	1276
6	IEPOX-SOA	0.53	235	OH	$2.5 x10^8$	46	4	1790
7	IEPOX-SOA	0.45	175	O_3	$6.0 x10^{13}$	50	4	24
8	IEPOX-SOA	0.51	220	O_3	$5.4 x10^{13}$	46	4	132
9	2-MTS	-	115	OH	$2.6 x10^8$	45	4	1274
10	2-MTS	-	105	OH	$5.3 x10^8$	51	4	1858

Ambient PM2.5 Collection. To confirm that potential new SOA tracers identified during smog chamber studies described above are atmospherically relevant, the experimental data were directly compared with field data collected during the 2013 Southern Oxidant and Aerosol Study (SOAS) at Look Rock, TN[26], during summer 2016 in downtown Manaus, Brazil, as part of the Green Ocean Amazon field campaign,[29] and during summer 2018 in the Galápagos Islands.[59] All three sites are in isoprene-rich regions and are typically under low-NO conditions. Further information about the collection and extraction of quartz filters can be found elsewhere.[16] Briefly, a 23-h aerosol sample (8 am 17 June–7 am 18 June, local time) collected from Look Rock, TN,

was selected for reanalysis by the HILIC/ESI-HR-QTOFMS method used in the present study, because it corresponds to the highest IEPOX-derived SOA mass measured by the Aerosol Chemical Speciation Monitor (ACSM, Aerodyne, Inc.). IEPOX-derived SOA as measured by the ACSM was resolved by positive matrix factorization (PMF) analysis.[26] A 24-h sample selected for reanalysis from Manaus, Brazil, was collected on 24 September 2016. This quartz filter sample was selected because it was minimally influenced by biomass burning as determined based on the lowest and highest measured concentrations of levoglucosan[70] and 2-MTSs,[29] respectively.

Aerosol Chemical Characterization. Both experimental and field filter samples (including field blanks and chamber blanks) were extracted in 20 mL of methanol (Optima LC/MS Grade, Fisher Scientific) by 45-min sonication. The methanol was dried under high-purity nitrogen (Airgas) and the extract reconstituted in 200 μL of 95:5 (v/v) solvent mixture of acetonitrile (ACN, HPLC grade, Fisher Scientific) and Milli-Q water. Filter extracts were chemically analyzed at the molecular level using HILIC/ESI-HR-QTOFMS operated in the negative ion mode (–), as recently described in detail by Cui et al.[29]. HILIC/(–)ESI-HR-QTOFMS data were analyzed by Agilent MassHunter Version B.06.00 Build 6.0.633.0 qualitative software (Agilent Technologies).

CHAPTER 3: RESULTS AND DISCUSSION

Time Series of Experiments. As shown in Figures 1a and 1b, the time series of representative 1- and 4-h heterogeneous •OH oxidation experiments of freshly-generated IEPOX-derived SOA (experiments 1 and 4, respectively, Table 1), the acidic $Sulf_{inorg}$ seed aerosol initially stabilized after 10 min of injection through atomization. At 120 and 90 min in Figures 1a and 1b, respectively, gas-phase IEPOX was injected into the chamber and upon becoming well-mixed, the SEMS volume concentration increased due to acid-catalyzed multiphase conversion of IEPOX into SOA constituents (as shown in Scheme 1). After 60 min of IEPOX injection, a filter was collected for 1 h, and then gas-phase •OH was introduced. During either 1- or 4-h of oxidative aging of freshly-generated IEPOX-derived SOA particles with •OH, the SEMS aerosol size distribution data indicated that the particles grew in size and decreased in concentration, consistent with expected coagulation and wall loss, respectively. If particles were shrinking due to offgassing of smaller volatile products produced the from fragmentation of the C_5-isoprene skeleton, this effect is negligible compared to coagulation. As a result, most of the SOA constituents formed during heterogeneous •OH oxidation of freshly-generated IEPOX-derived SOA appear to remain within the particle for the length of the experiments. Similarly, we can largely rule out gas-phase reaction of IEPOX with •OH as a contributor to the particle volume (or mass), as particle growth is not noticeably faster than it would be due to coagulation. The 2-MTS •OH oxidation experiments showed a similar trend.

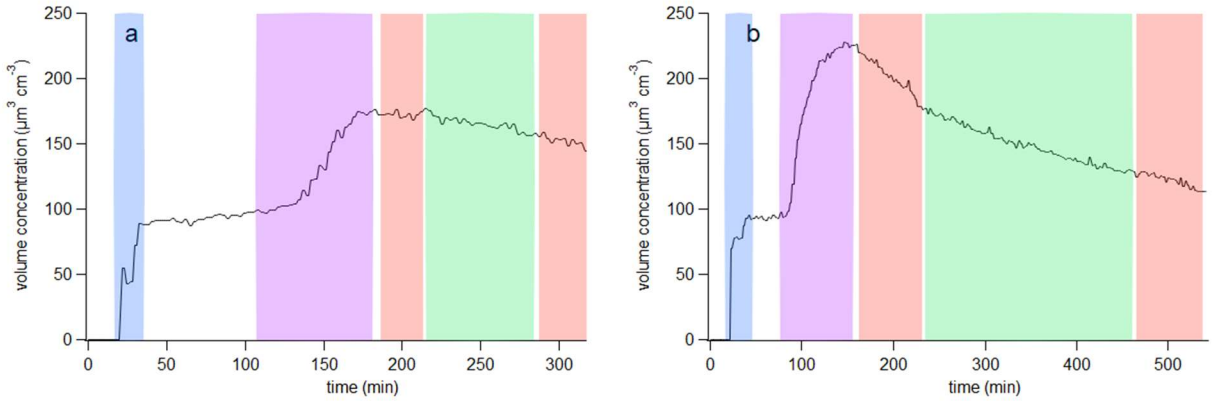

Figure 1. Time series of aerosol volume concentrations for 1-h (experiment 1, Table 1) (a) and 4-h (experiment 4, Table 1) (b) heterogeneous •OH oxidation experiments of freshly-generated IEPOX-derived SOA. Blue regions mark seed injection; purple regions mark IEPOX injection; red regions mark filter collections; green regions are during heterogeneous •OH oxidation.

Proposed Reaction Schemes. Scheme 1 shows proposed reaction mechanisms leading to the formation of freshly-generated IEPOX-derived SOA constituents (2-MTs, 2-MTSs, and the 2-MTS dimers with the corresponding $[M–H]^-$ ion at *m/z* 333 ($C_{10}H_{21}O_{10}S^-$)). Schemes 2, 3, and 4 show proposed heterogeneous •OH oxidation mechanisms for 2-MTSs, 2-MTs, and the 2-MTS dimers, respectively. IEPOX predominantly transforms into 2-MTs and 2-MTSs through its acid-driven multiphase chemistry within the aqueous $Sulf_{inorg}$ phase;[9,10,16,29] however, these studies have also shown that OS dimers at *m/z* 333 ($C_{10}H_{21}O_{10}S^-$) are present.

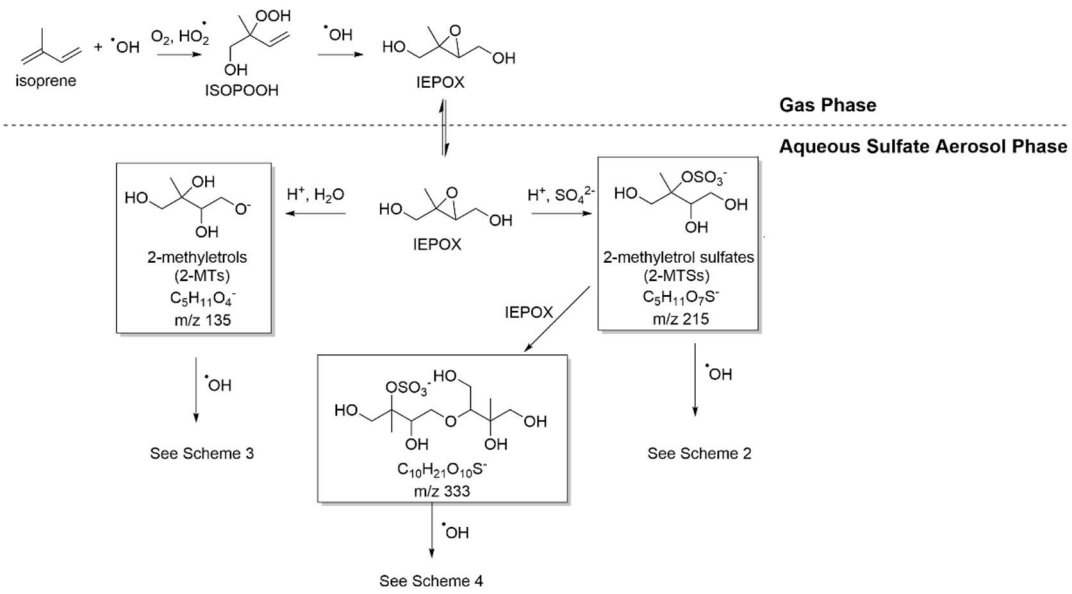

Scheme 1. •OH -initiated oxidation of isoprene to IEPOX, followed by acid-driven reactive uptake of IEPOX into the aqueous $Sulf_{inorg}$ particle phase yielding freshly-generated SOA tracers detected by HILIC/(–)ESI-HR-QTOFMS, including 2-MTs and 2-MTSs as well as the 2-MTS dimers measured as the $[M–H]^-$ ion at *m/z* 333 ($C_{10}H_{21}O_{10}S^-$).

Particulate 2-MTSs and 2-MTs may both be oxidized by •OH at one of four sites by hydrogen abstraction, labelled 1-4 in Schemes 2 and 3, respectively. Although we did not directly determine the heterogeneous •OH oxidation rate constants in the present study, we recently obtained the effective second-order heterogeneous OH oxidation rate constant for 2-MTS aerosols as $4.9\pm0.6\times10^{-13}$ cm^3 $molecule^{-1}$ s^{-1} by using an oxidation flow reactor (OFR).[59] By assuming an average ambient •OH concentration of 1.5×10^6 molecules cm^{-3}, we estimated from this recent study that the atmospheric lifetime (τ) of particulate 2-MTSs against OH oxidative aging was ~16±2 days, which was comparable to 16±3 days and 19±9 days determined for particulate 3-MTSs,[46] the minor MTS isomers, and IEPOX-derived SOA,[58] respectively. Since accumulation mode sulfate aerosols typically have atmospheric lifetimes of 2 weeks,[71] the heterogeneous •OH oxidation of IEPOX-derived SOA could be an important chemical sink that may need to be

considered in atmospheric chemistry models, especially when •OH levels are enhanced in urban areas.[72] Our results presented here are focused on chemically characterizing products in Schemes 2, 3, and 4 from the heterogeneous •OH oxidation of 2-MTSs, 2-MTs, and the 2-MTS dimers, respectively, by using HILIC/(–)ESI-HR-QTOFMS. Although heterogeneous •OH oxidation mechanisms were recently proposed for particulate 2-MTSs,[59] our present study aimed to examine this process with the entire IEPOX-SOA mixture and at longer reaction timescales and lower •OH concentrations than used in prior studies. In addition, our combination of chamber-generated and ambient aerosol samples help to demonstrate feasibility of heterogeneous •OH oxidation of IEPOX-derived SOA in the atmosphere, and thus, likely yield new SOA markers of atmospheric oxidative aging of IEPOX-derived SOA.

Scheme 1 and Table 2 show that 2-MTSs are present in non-aged (freshly-generated) IEPOX-derived SOA. Since 2-MTSs are known to be the most abundant IEPOX-derived SOA tracers and OSs measured in atmospheric aerosols[7,9,10,29,53] and we measured these in our freshly-generated IEPOX-derived SOA, we proposed that the heterogeneous •OH -initiated oxidation of particulate 2-MTSs occurs during our 1- and 4-h oxidative aging experiments. The proposed pathways shown in Scheme 2 are the same as those recently proposed by Chen et al.[59] At longer reaction timescales and lower •OH concentrations utilized in the present study compared to those of Chen et al.,[59] we observe all the aged and multifunctionalized OSs previously reported. Briefly, the regiochemistry of the RO_2 intermediates dictates the structures of the OS products shown in Scheme 2 via Russell disproportionation,[73] Bennett-Summers reaction,[74] or β-scission.[75,76] This is discussed in more detail in that study,[59] but we will apply this in detail below for the 2-MTSs.

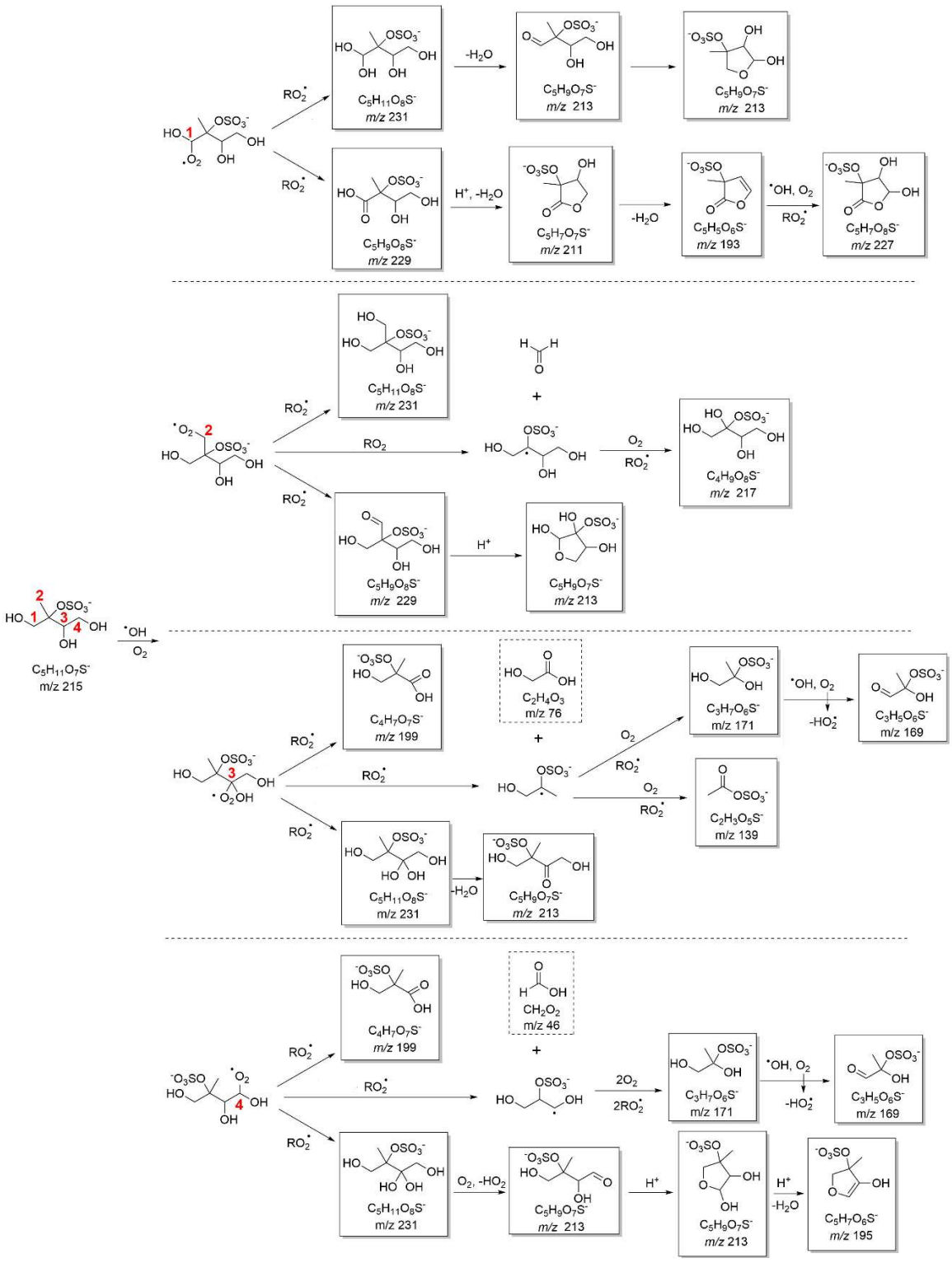

Scheme 2. Proposed heterogeneous •OH oxidation of particulate 2-MTSs. Each pathway from one oxidation site at carbons labelled 1, 2, 3, or 4 is divided by a dotted line. Dotted boxes mark species that were not detected in the final (4-h) mixture but could be below HILIC/(–)ESI-HR-QTOFMS detection limits; solid boxes mark species detected in this study by HILIC/(–)ESI-HR-QTOFMS.

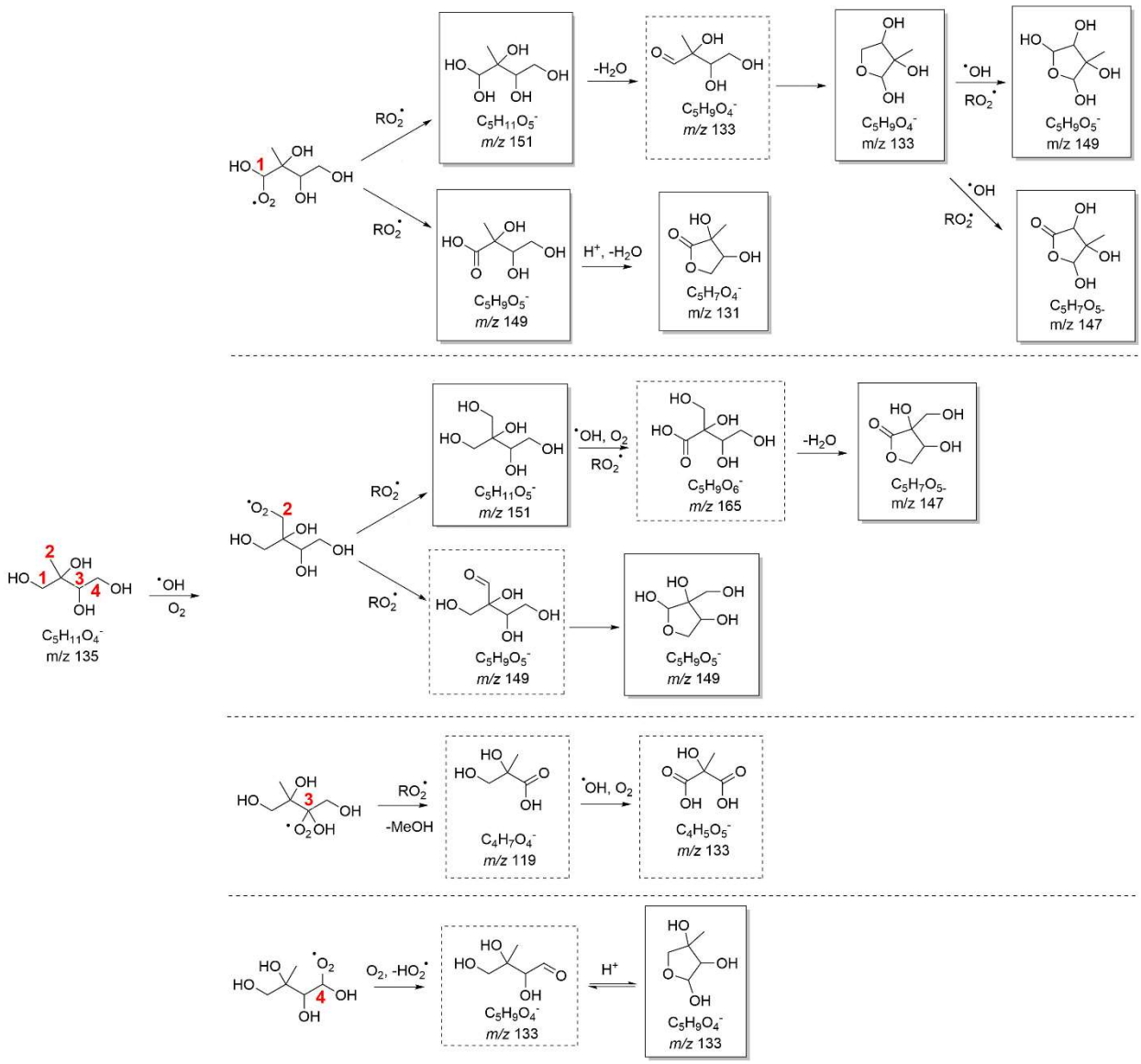

Scheme 3. Proposed heterogeneous OH oxidation of 2-MTs. Each pathway from one oxidation site at carbons labelled 1, 2, 3, or 4 is divided by a dotted line. Dotted boxes mark species that were not detected in the final (4-h) mixture but may be below HILIC/(–)ESI-HR-QTOFMS detection limits; solid boxes mark species detected in this study by HILIC/(–)ESI-HR-QTOFMS.

The heterogeneous •OH oxidation of 2-MTs is similar in many ways to the 2-MTSs: Russell disproportionation or hydroperoxy radical (HO_2) elimination[77,78] of C_1- and C_4-RO_2 intermediates shown in Scheme 3 leads to C_5 γ-hydroxy aldehydes that cyclize to C_5-hemiacetals detected at *m/z* 133 ($C_5H_9O_4^-$), while the Bennett-Summers reaction of the same RO_2 intermediates

leads to lactones detected at *m/z* 131 ($C_5H_7O_4^-$) through dehydration of γ-hydroxy carboxylic acids ($C_5H_{10}O_5$) via acid-catalyzed Fischer esterification.[79-81] The precursor γ-hydroxy carbonyl compounds are not typically observed by mass spectral techniques.[82] Ions at *m/z* 149 ($C_5H_9O_5^-$) could also form from the Bennett-Summers reaction of the C_2-RO_2 intermediate shown in Scheme 3 that forms a C_5 γ-hydroxy aldehyde, which then cyclizes to yield a C_5-hemiacetal isomer detected at *m/z* 149 ($C_5H_9O_5^-$). The lactone at *m/z* 147 ($C_5H_7O_5^-$) forms in similar reactions that differ only by regiochemistry, and the pentol at *m/z* 151 ($C_5H_{11}O_5^-$) is a first-generation oxidation product from 2-MTs. These compounds—the ions at *m/z* 131($C_5H_7O_4^-$), 133 ($C_5H_9O_4^-$), 147 ($C_5H_7O_5^-$), 149 ($C_5H_9O_5^-$), and 151 ($C_5H_{11}O_5^-$) — are observable in both chamber-generated SOA and atmospheric SOA taken from the southeastern United States and Manaus, Brazil (Figure 2), and have not been extensively studied. As such, there are no previously published reaction pathways for these compounds.

Figure 2 shows extracted ion chromatograms (EICs) for these five non-OS compounds in an SOA sample collected from a 4-h heterogeneous $^{\bullet}OH$ oxidation experiment of freshly-generated IEPOX-derived SOA (experiment 4) and from an atmospheric aerosol sample collected from the Galápagos Islands. The signal strengths for these compounds are low compared to the OSs, but RTs of chamber samples and ambient samples are consistent; for *m/z* 133 ($C_5H_9O_4^-$), RTs for 4 out of the 6 visible chromatographic peaks (isomers: RT 1.98, 2.17, 2.29, and 4.58 min) correspond exactly, and for other *m/z* values (or SOA constituents) some chromatographic peaks are shared between the chamber-generated and ambient SOA sample. This supports that the chamber-generated SOA likely contains the same compounds and isomers found in ambient $PM_{2.5}$.

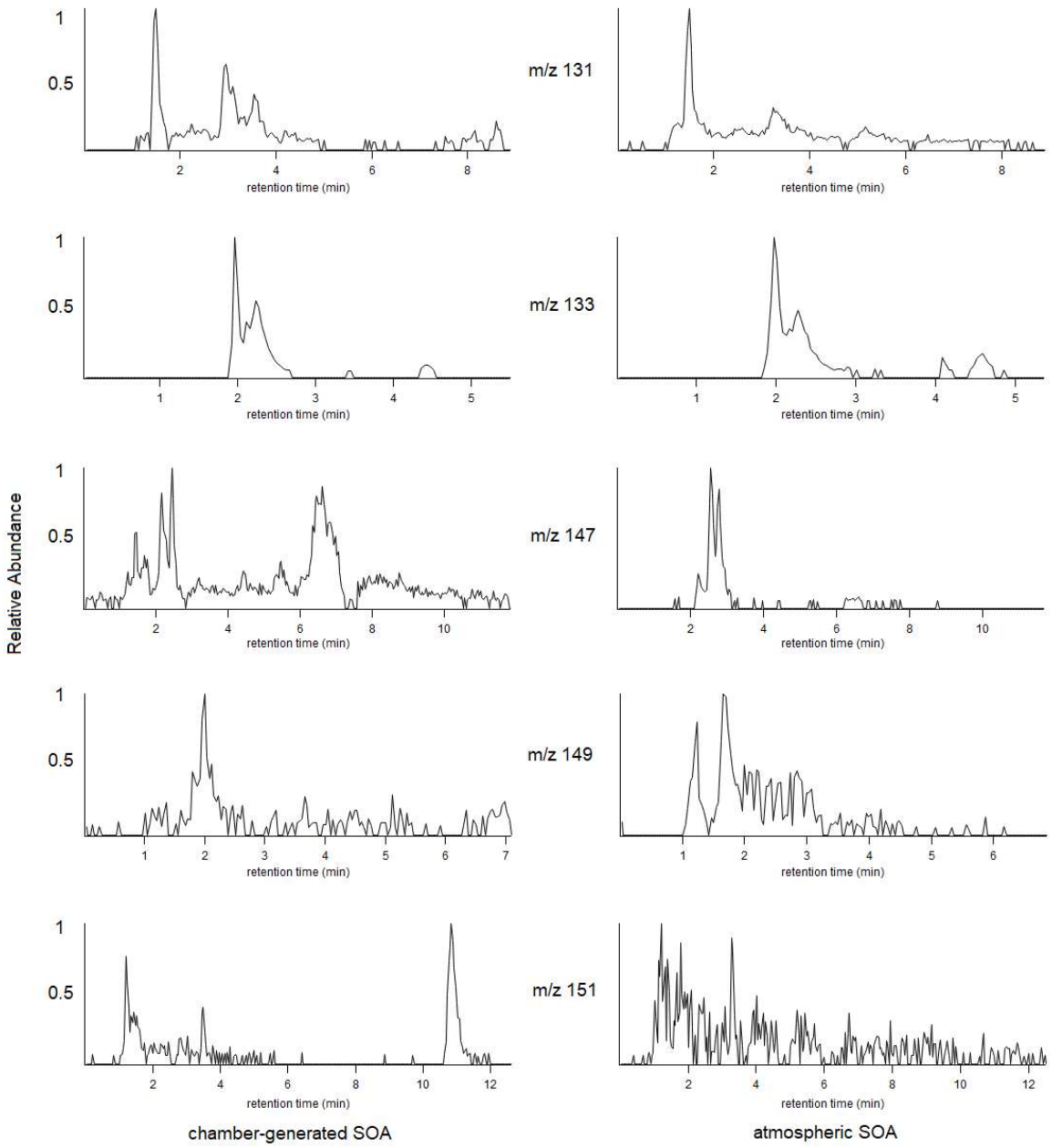

Figure 2. EICs comparing chamber-generated IEPOX-derived SOA heterogeneously aged by OH for 4 h (left panels) to $PM_{2.5}$ collected from Galápagos Islands, Ecuador (right panels), for $[M–H]^-$ ions detected at *m/z* 131 ($C_5H_7O_4^-$), 133 ($C_5H_9O_4^-$), 147 ($C_5H_7O_5^-$), 149 ($C_5H_9O_5^-$), and 151 ($C_5H_{11}O_5^-$). Each EIC signal is normalized to the maximum peak height for each sample.

Schemes 4a-c show possible reaction pathways for heterogeneous •OH oxidation of one isomer for the dimers detected as $[M–H]^-$ ions at *m/z* 333 ($C_{10}H_{21}O_{10}S^-$) at four of the eight carbon

sites that have abstractable hydrogens. These pathways are proposed based on similarities to the structures of 2-MTs and 2-MTSs, and are supported by the detection of $[M–H]^-$ ions at *m/z* 243 ($C_6H_{11}O_8S^-$), 273 ($C_7H_{13}O_9S^-$), 275 ($C_7H_{15}O_9S^-$), 285 ($C_8H_{13}O_9S^-$), 329 ($C_{10}H_{17}O_{10}S^-$), and 331 ($C_{10}H_{19}O_{10}S^-$) in both chamber-generated and ambient SOA (Figures 3a-b). Previous studies[32,83] have found evidence in ambient SOA (or cloud water samples) for *m/z* 317 ($C_9H_{17}O_{10}S^-$), 331 ($C_{10}H_{19}O_{10}S^-$), and 333 ($C_{10}H_{21}O_{10}S^-$) (included in Schemes 4 a-c), as well as *m/z* 279 ($C_{10}H_{15}O_7S^-$), 281 ($C_{10}H_{17}O_7S^-$), and 283 ($C_{10}H_{19}O_7S^-$), which may also be products of heterogeneous $^{\bullet}OH$ oxidation of *m/z* 333 based on their formulas. Due to their C_6-C_{10} backbones, past studies may have misidentified these as monoterpene-derived OSs.[83] Ions at *m/z* 303 ($C_8H_{15}O_{10}S^-$), 317 ($C_9H_{17}O_{10}S^-$), and 319 ($C_9H_{19}O_{10}S^-$) were not detected in the 3 atmospheric $PM_{2.5}$ samples analyzed in this study, although they were detected in chamber-generated SOA, indicating that perhaps ambient levels were below the limit of detection of HILIC/(–)ESI-HR-QTOFMS.

Figures 3a and 3b compare chamber-generated IEPOX-derived SOA to atmospheric $PM_{2.5}$. Elution times between chamber and atmospheric samples differ by up to 0.5 min because they were analyzed on different days, but many of the ions under *m/z* 300 have a clear correspondence between chamber and atmospheric samples. However, atmospheric samples for *m/z* 299, 301, 329, and 331 are less clear, and it would be beneficial to analyze more concentrated atmospheric $PM_{2.5}$ samples to confirm the relevance of these compounds.

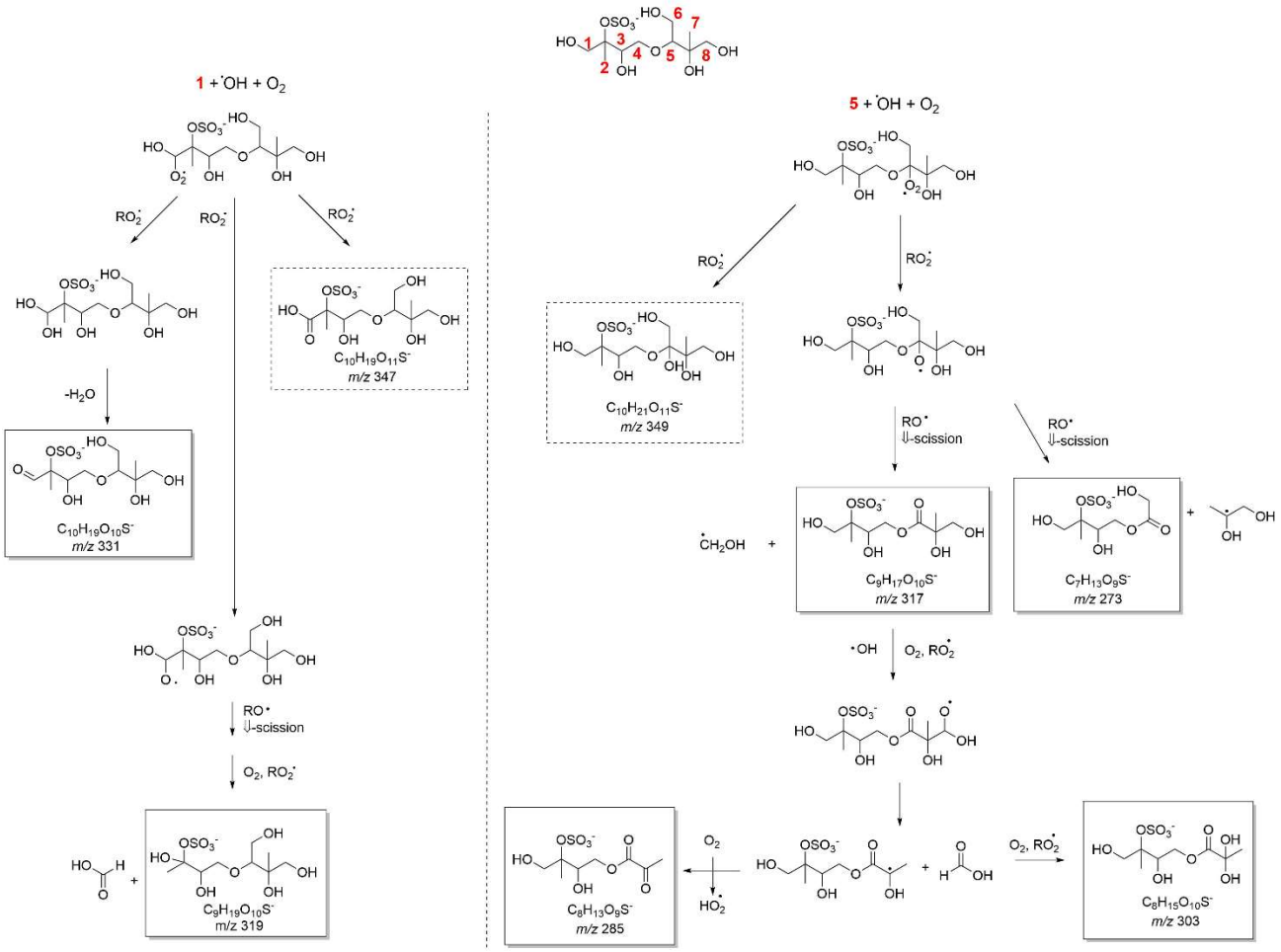

Scheme 4a. Proposed reaction scheme for heterogeneous •OH oxidation of the carbons labelled 1 and 5 on one isomer of the dimer detected at *m/z* 333, divided by a dotted line. Dotted boxes mark species that were not detected in the final (4-h) mixture, but may be below HILIC/(–)ESI-HR-QTOFMS detection limits; solid boxes mark species detected in this study by HILIC/(–)ESI-HR-QTOFMS.

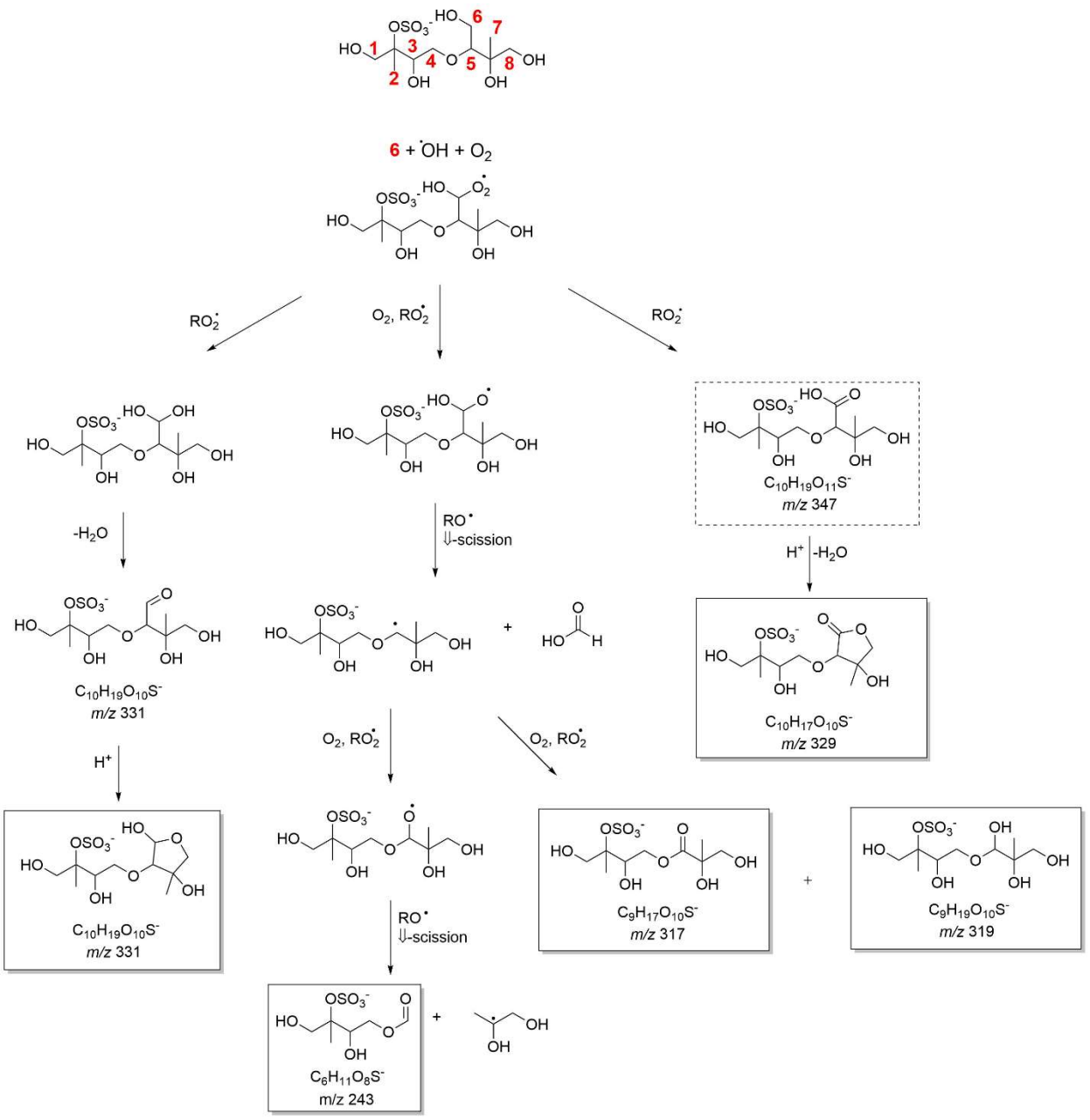

Scheme 4b. Proposed reaction scheme for heterogeneous •OH oxidation of the carbon labelled 6 on one isomer of the dimer detected at *m/z* 333. Dotted boxes mark species that were not detected in the final (4-h) mixture, but may be below HILIC/(–)ESI-HR-QTOFMS detection limits; solid boxes mark species detected in this study by HILIC/(–)ESI-HR-QTOFMS.

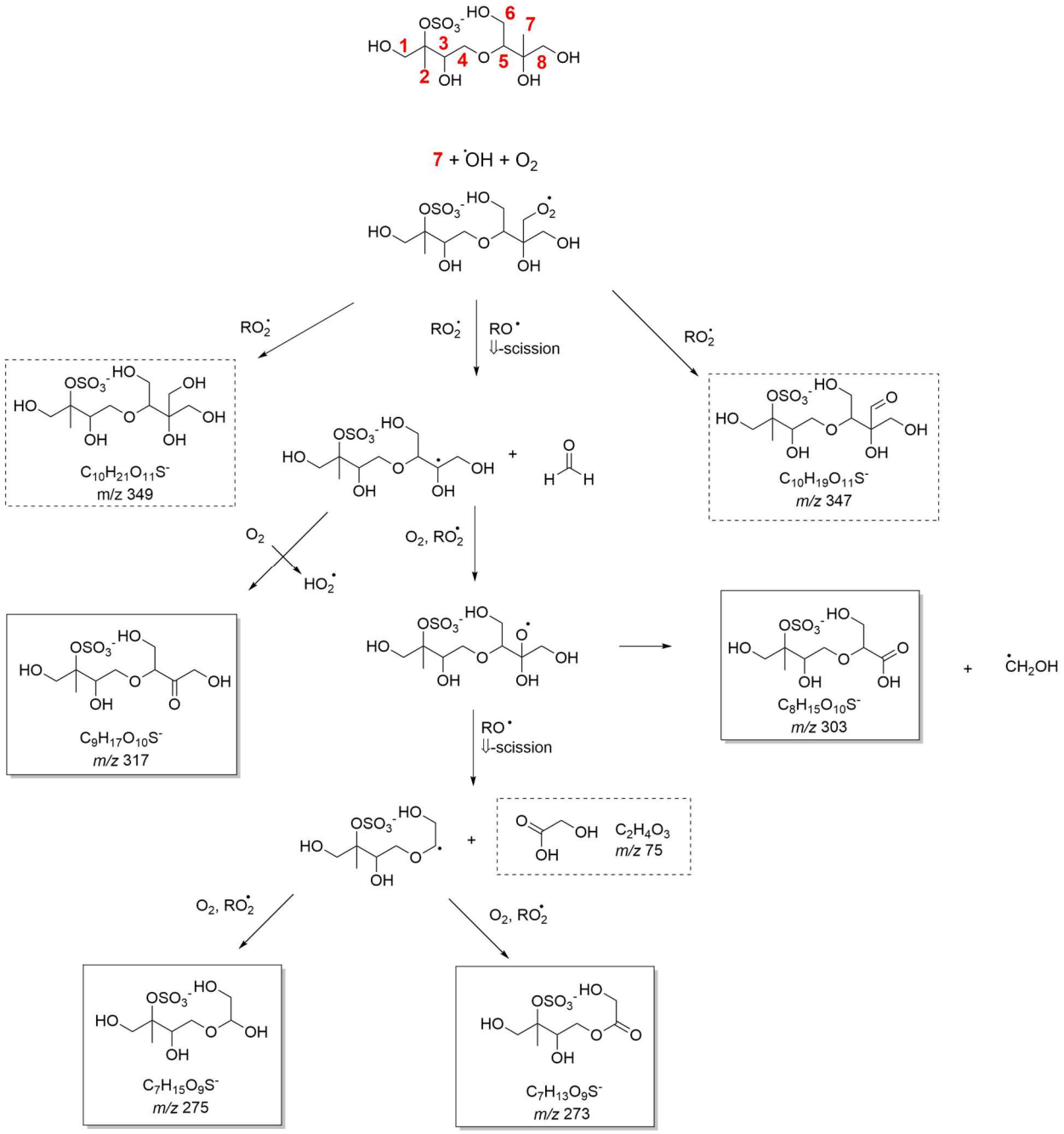

Scheme 4c. Proposed reaction scheme for heterogeneous •OH oxidation of the carbon labelled 7 on one isomer of the dimer detected at *m/z* 333. Dotted boxes mark species that were not detected in the final (4-h) mixture, but may be below HILIC/(–)ESI-HR-QTOFMS detection limits; solid boxes mark species detected in this study by HILIC/(–)ESI-HR-QTOFMS.

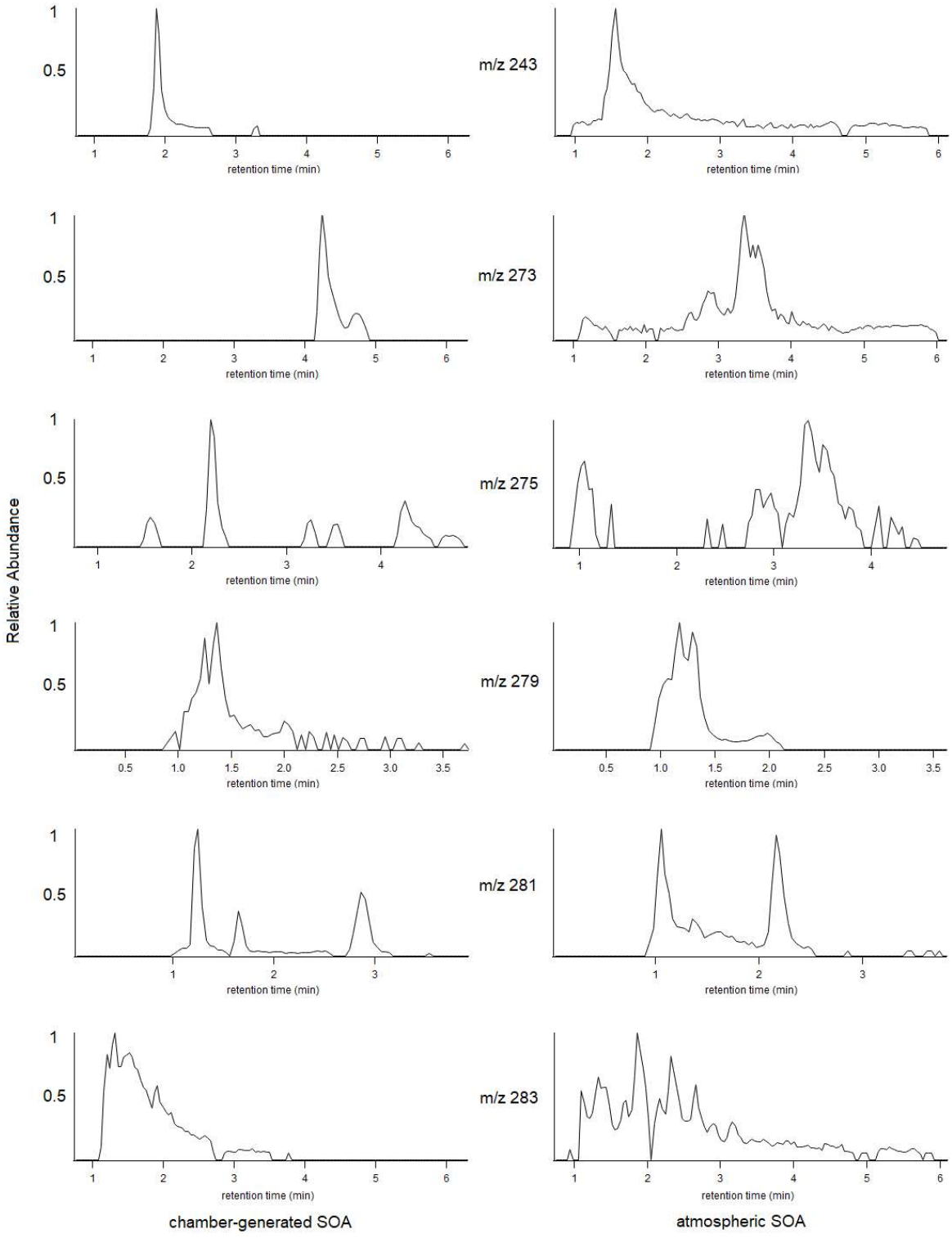

Figure 3a. EICs comparing chamber-generated IEPOX-derived SOA heterogeneously aged by •OH for 4 h (left panels) to $PM_{2.5}$ collected from Galápagos Islands, Ecuador (right panels), for $[M–H]^-$ ions detected at *m/z* 243 ($C_6H_{11}O_8S^-$), 273 ($C_7H_{13}O_9S^-$), 275 ($C_7H_{15}O_9S^-$), 279 ($C_{10}H_{15}O_7S^-$), 281 ($C_{10}H_{17}O_7S^-$), and 283 ($C_{10}H_{19}O_7S^-$). Each EIC signal is normalized to the maximum peak height for each sample.

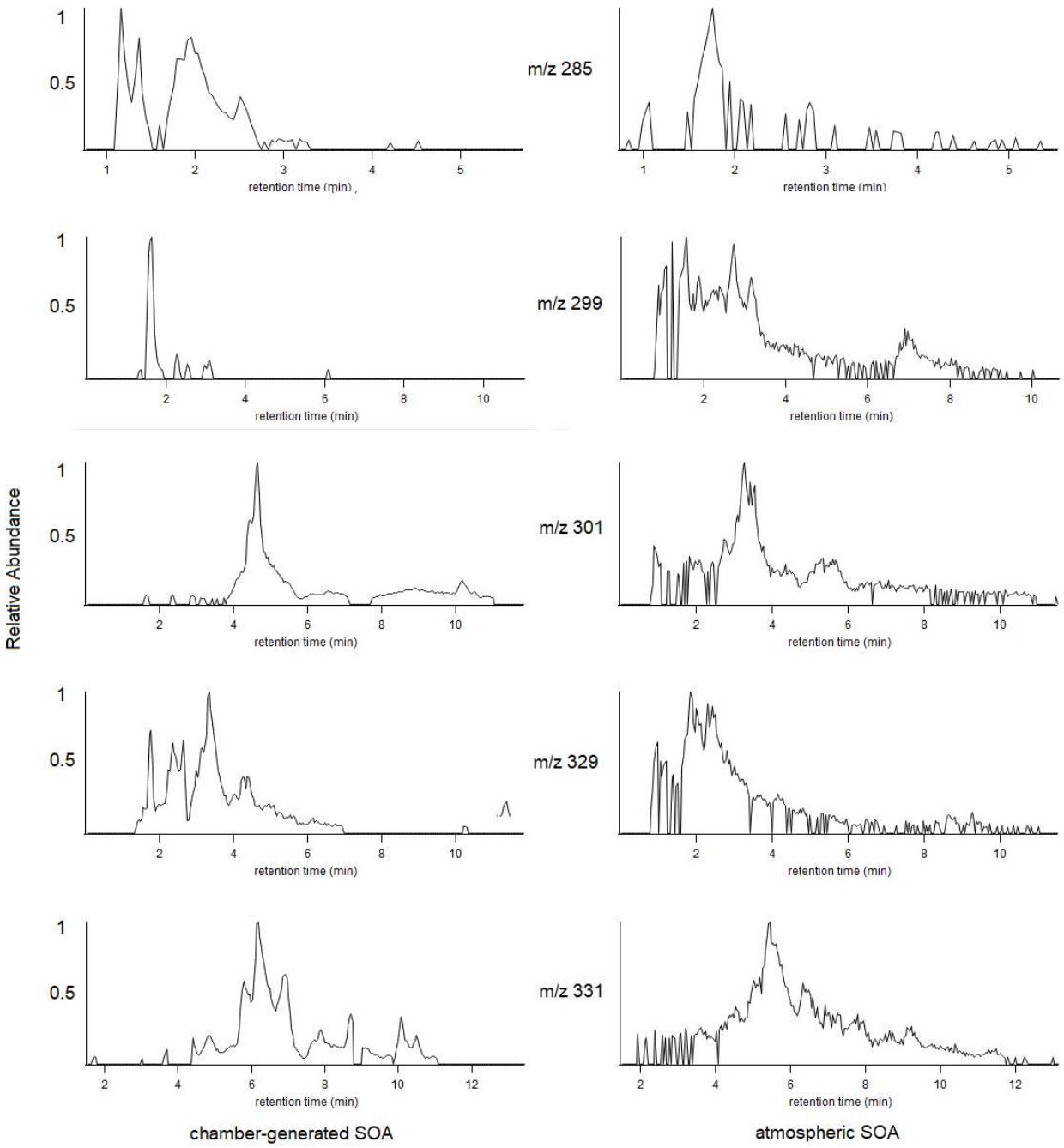

Figure 3b. EICs comparing chamber-generated IEPOX-derived SOA heterogeneously aged by OH for 4 h (left panels) to $PM_{2.5}$ collected from Galápagos Islands, Ecuador (right panels), for $[M–H]^-$ ions detected at *m/z* 285 ($C_8H_{13}O_9S^-$), 299 ($C_{10}H_{19}O_8S^-$), 301 ($C_8H_{13}O_{10}S^-$), 329 ($C_{10}H_{17}O_{10}S^-$), and 331 ($C_{10}H_{19}O_{10}S^-$). Each EIC signal is normalized to the maximum peak height for each sample.

Production and Consumption of Tracers. Production and consumption of tracked SOA constituents are ranked by fold change rather than difference. Authentic standards are not available for most of these SOA constituents, meaning that the relative ionization efficiency is unknown and an equivalent difference in ion count for two compounds may indicate a drastically different amount of change in aerosol mass concentration. Fold change does have a disadvantage in that a compound that was not present above the limit of quantification for the mass spectrometer may appear to have a very large fold change for a small total amount of production. For this reason, a table noting ions with 'significant presence' (peak area > 100,000 ion counts) before aging is also included. 'Significant fold change' is defined as fold change >3.

Pre-Aging Samples. Table 2 shows SOA tracers significantly present in freshly-generated IEPOX-derived SOA before heterogeneous •OH oxidation, but not present in the 2-MTSs standard (i.e., not a contaminant). In addition to their formation from IEPOX, 2-MTs may form from hydrolysis of 2-MTSs,[84,85] and the reaction between 2-MTSs and IEPOX forms the dimer detected by HILIC/(–)ESI-HR-QTOFMS at *m/z* 333;[83] *m/z* 197 ($C_5H_9O_6S^-$) is likely produced from the dehydration of 2-MTSs.

Table 2. Compounds found in freshly-generated (non-aged by heterogeneous OH oxidation) IEPOX-derived SOA.

Theoretical m/z ([M-H]$^-$)	Empirical formula	DBE[a]	O:C	Tentatively Proposed Structure[b]	RT[c] (min)	Mass error (mDa)	Parent Compound and Generation[d]
133.051	$C_5H_9O_4^-$	1	0.8	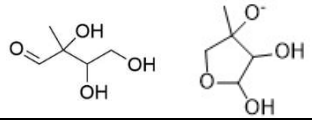	1.96 2.24 4.46	+0.2 +0.2 +0.3	2-MTs; 1
135.066	$C_5H_{11}O_4^-$	0	0.8	2-MTs	1.75 3.00 4.42	+0.1 +0.0 +0.2	IEPOX; 0
138.970	$C_2H_3O_5S^-$	1	2.5	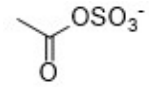	1.13 6.91 7.50	+0.0 +0.1 +0.1	2-MTSs; 3
147.030	$C_5H_7O_5^-$	2	1	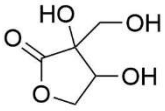	1.42 2.19 2.43 6.47	+0.0 -0.2 -0.4 -0.3	2-MTs; 2
170.997	$C_3H_7O_6S^-$	0	2	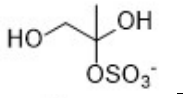	6.11 8.80	-0.2 +0.1	2-MTSs; 3
197.013	$C_5H_9O_6S^-$	1	1.2	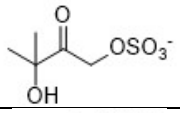	1.88 5.09 7.90	+0.1 -0.2 -0.5	2-MTSs; 0
210.991	$C_5H_7O_7S^-$	2	1.4	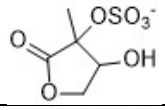	1.05 1.45 1.72	+0.7 +0.2 +0.9	2-MTSs; 1
213.007	$C_5H_9O_7S^-$	1	1.4	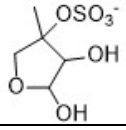	2.11 4.87	+0.9 +1.1	2-MTSs; 1
215.023	$C_5H_{11}O_7S^-$	0	1.4	2-MTSs	2.10 4.23 5.76	+0.3 +0.5 +0.4	IEPOX; 0
243.018	$C_6H_{11}O_8S^-$	1	1.3	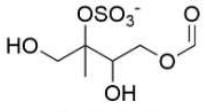	1.48 1.90 3.25 4.59	+0.2 +0.1 -0.4 +0.2	m/z 333; 5
281.070	$C_{10}H_{17}O_7S^-$	2	0.7	?	2.98	+0.1	m/z 333; ?
303.039	$C_8H_{15}O_{10}S^-$	1	1.3	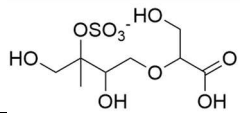	2.61 4.64	+0.7 +1.96	m/z 333; 3,5
317.055	$C_9H_{17}O_{10}S^-$	1	1.1	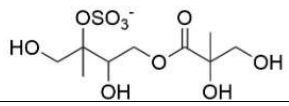	4.77	+3.2	m/z 333; 3,4
319.070	$C_9H_{19}O_{10}S^-$	0	1.1	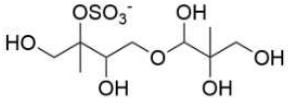	1.46 1.65	+6.4 +2.0	m/z 333; 3,4

333.086	$C_{10}H_{21}O_{10}S^-$	0	1	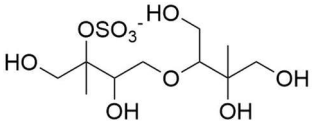	10.65 11.51 13.33 16.68 17.09	+0.2 +0.0 +0.3 +0.3 +0.1	2-MTSs, IEPOX; 0

[a] DBE = double bond/ring equivalent
[b] Only one structural isomer each for ring and chain structures is shown
[c] RT = retention time
[d] Oxidative generation is the number of reactions during which more oxygens have been added since the parent compound

The SOA tracers produced significantly during IEPOX reactive uptake before aging were similar in identity to those in the 2-MTS seed aerosols. This stands in contrast to a recent oxidation flow reactor study done with 2-MTSs as a starting reactant,[59] which found no additional compounds other than impurities in the standard. However, residence and filter collection times in the present study were much longer (~2.5 hours compared to ~0.5 hours), allowing slower reactions to take place. There may be alternate and much slower pathways that produce different isomers than heterogeneous •OH oxidation, such as dark Fenton reactions.[86]

IEPOX-SOA aging experiments with OH. Figure 4 compares geometric mean fold change for SOA constituents in the 1-h and 4-h heterogeneous •OH oxidation experiments of freshly-generated IEPOX-derived SOA, corrected for chamber dilution and filter through volume. The ions with significantly higher fold production in the 1-h than the 4-h experiments, which implies consumption over the remaining 3 h, are *m/z* 131 ($C_5H_7O_4^-$) and 281 ($C_{10}H_{17}O_7S^-$). The other prominent ions produced during the 1-h heterogeneous OH oxidation experiments of freshly-generated IEPOX-derived SOA are *m/z* 211 ($C_5H_7O_7S^-$), 229 ($C_5H_9O_8S^-$), 273 ($C_7H_{13}O_9S^-$) and 281 ($C_{10}H_{17}O_7S^-$). As was expected based on Schemes 2-4, 2-MTs, 2-MTSs, and the 2-MTS dimers all decreased during the heterogeneous •OH oxidation experiments of freshly-generated IEPOX-derived SOA, and the consumption was more pronounced at 4-h of heterogeneous •OH oxidation. In fact, these 3 precursors were the most consumed during heterogeneous •OH

oxidation of freshly-generated IEPOX-derived SOA.

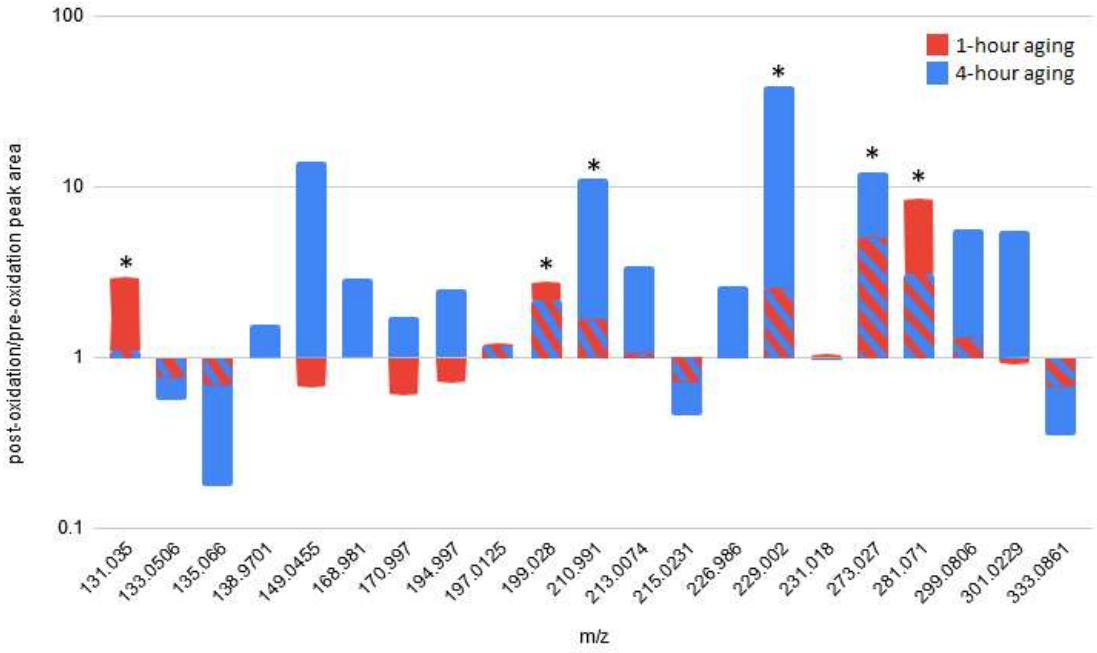

Figure 4. Comparison of geometric mean fold change (EIC peak area from post-oxidation filter/EIC peak area from pre-oxidation filter) for 21 selected $[M–H]^-$ ions from three 1-h heterogeneous •OH oxidation experiments of freshly-generated IEPOX-derived SOA (red) and three 4-h heterogeneous •OH oxidation experiments of freshly-generated IEPOX-derived SOA (blue). Color bars are overlaid rather than added to each other, and the striped region represents both red and blue bars. Asterisks denote ions described in the text.

Given two separate time points showing consistency across multiple experiments, it can be assumed that the five ions (or SOA constituents) produced significantly during the 1-h oxidative aging experiments are among the first- and second-generation products from heterogeneous •OH oxidation of freshly-generated IEPOX-derived SOA. The nine additional ions (or SOA constituents) produced during 4-h oxidative aging experiments may be later-generation SOA constituents or those formed from slower early-generation reactions. These could also be SOA constituents produced during acid-driven reactive uptake of IEPOX in the aqueous $Sulf_{inorg}$ phase,

partitioned to the surface of the particle, and then consumed during heterogeneous •OH oxidation. Table 3 shows SOA constituents with significant fold changes during the 1-h oxidative aging experiments, and Table 4 shows SOA constituents with significant fold changes during the 4-h oxidative aging experiments. Not included in Tables 3 and 4 are the tracked ions *m/z* 279 ($C_{10}H_{15}O_7S^-$), 283 ($C_{10}H_{19}O_7S^-$), and 319 ($C_9H_{19}O_{10}S^-$), which were not significantly present either before or after heterogeneous •OH oxidation. This may indicate unfavorable branching ratios or reaction conditions, and bears further investigation.

Table 3. Compounds with fold changes > 3 in the 1-h heterogeneous •OH oxidation experiments of freshly-generated IEPOX-derived SOA.

Theoretical m/z ([M-H]$^-$)	Empirical formula	DBE[a]	O:C	Tentatively Proposed Structure[b]	RT[c] (min)	Mass error (mDa)	Parent Compound and Generation[d]
131.035	$C_5H_7O_4^-$	2	0.8	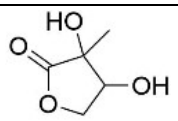	1.49 2.99 8.61 14.98	+5 +3 +5 +6	2-MTs; 2
229.002	$C_5H_9O_8S^-$	1	1.6	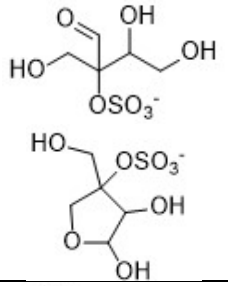	2.43 2.89 3.71 3.89	+0.0 +0.1 -0.1 +0.1	2-MTSs; 1,2
273.029	$C_7H_{13}O_9S^-$	1	1.3	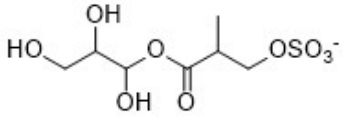	4.25 4.79 23.45	+0.0 +0.0 +0.4	2-MTSs; ?
281.070	$C_{10}H_{17}O_7S^-$	2	0.7	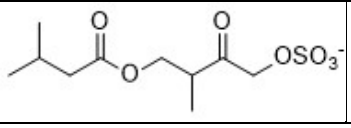	2.98	+0.1	2-MTS dimers; ?

[a] DBE = double bond/ring equivalent
[b] Only one structural isomer each for ring and chain structures is shown
[c] RT = retention time
[d] Oxidative generation is the number of reactions during which more oxygens have been added since the parent compound

The four ions consumed during both 1-h and 4-h oxidative aging experiments are *m/z* 133

($C_5H_9O_4^-$), 135 (2-MTs), 215 (2-MTSs), and 333 ($C_{10}H_{21}O_{10}S^-$); these compounds are precursors to the ions produced during heterogeneous •OH oxidation of the SOA mixture. Tables 3 and 4 show compounds produced significantly (fold change > 3) from these precursors, as detailed in Schemes 2-4.

Table 4. Compounds with fold changes > 3 in the 4-h heterogeneous •OH oxidation experiments of freshly-generated IEPOX-derived SOA.

Theoretical m/z ([M-H]$^-$)	Empirical formula	DBE[a]	O:C	Tentatively Proposed Structure[b]	RT[c] (min)	Mass error (mDa)	Parent Compound and Generation[d]
149.045	$C_5H_9O_5^-$	1	1	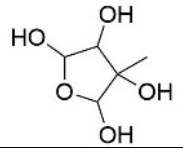	1.99	+5.0	2-MTs; 3
168.992	$C_3H_5O_6S^-$	1	2	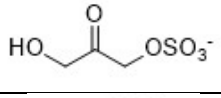	1.25 2.48	-3.5 -5.7	2-MTSs; 4
194.997	$C_5H_7O_6S^-$	2	1.2	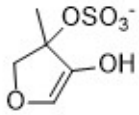	1.09 1.25	-0.2 +0.0	2-MTSs; 3
210.992	$C_5H_7O_7S^-$	2	1.4	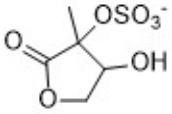	1.05 1.45 1.72 2.74 3.61	+0.7 +0.2 +0.9 +0.7 -0.2	2-MTSs; 2
213.007	$C_5H_9O_7S^-$	1	1.4	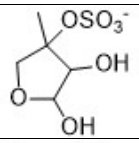	2.11 4.87	+0.9 +1.1	2-MTSs; 1
229.002	$C_5H_9O_8S^-$	1	1.6	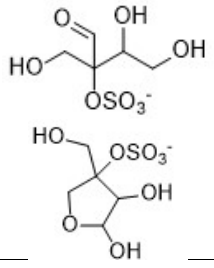	2.43 2.89 3.71 3.89	+0.0 +0.1 -0.1 +0.1	2-MTSs; 1, 2
231.018	$C_5H_{11}O_8S^-$	0	1.6	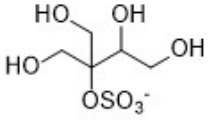	7.65	-0.3	2-MTSs; 2

243.018	$C_6H_{11}O_8S^-$	1	1.3	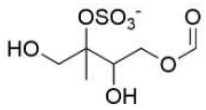	1.48 1.90 3.25 4.59	+0.2 +0.1 -0.4 +0.2	2-MTS dimers; 5
273.029	$C_7H_{13}O_9S^-$	1	1.3	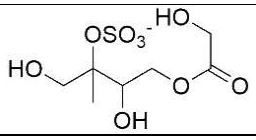	4.25 4.79 23.45	+0.0 +0.0 +0.4	2-MTS dimers; 3
275.044	$C_7H_{15}O_9S^-$	0	1.2	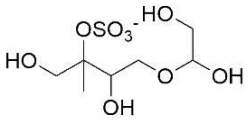	1.58 2.19 3.24 3.52 4.23 4.72	+0.2 -0.2 -0.2 -0.3 -0.2 -0.1	2-MTS dimers; 5
281.070	$C_{10}H_{17}O_7S^-$	2	0.7	?	2.98	+0.1	2-MTS dimers; ?
285.029	$C_8H_{13}O_9S^-$	2	1.1	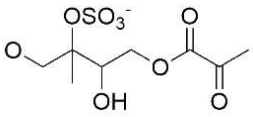	1.17 1.36 1.97 2.54	+0.4 +1.4 +1.2 +0.4	2-MTS dimers; 5
299.081	$C_{10}H_{19}O_8S^-$	1	0.8	?	1.63 2.27 2.51 3.11	-4.3 -0.5 +0.0 +2.2	2-MTS dimers; ?
301.023	$C_8H_{13}O_{10}S^-$	2	1.3	?	1.76 2.38	+1.0 +1.2	2-MTSs; ?
303.039	$C_8H_{15}O_{10}S^-$	1	1.3	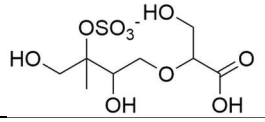	1.56 2.61 4.64	+0.5 +0.7 +1.96	2-MTS dimers; 3,5
329.055	$C_{10}H_{17}O_{10}S^-$	2	1	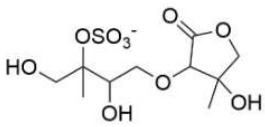	1.76 2.30 2.72 3.38 4.22 4.47	-0.2 +0.4 +0.8 +0.1 +0.1 +0.1	2-MTS dimers; 2
331.070	$C_{10}H_{19}O_{10}S^-$	1	1	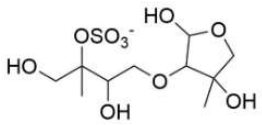	4.86 5.78 6.18 6.91 7.87 10.03	+0.2 +0.3 +0.4 +0.1 +0.7 +0.0	2-MTS dimers; 2

[a] DBE = double bond/ring equivalent
[b] Only one structural isomer each for ring and chain structures is shown
[c] RT = retention time
[d] Oxidative generation is the number of reactions during which more oxygens have been added since the parent compound

Ozone control. In the ozone control experiments, there is less production of all species produced during the heterogeneous •OH oxidation experiments. It is assumed that all SOA constituents with a high fold change in the control experiments are produced by internal, possibly acid-catalyzed reactions rather than heterogeneous oxidation by ozone. As shown in Table 1, ozone consumption is negligible compared to •OH consumption during heterogeneous •OH oxidation experiments.

Figure 5 shows geometric mean fold change for tracers in the control experiments, compared to 4-h heterogeneous OH oxidation of freshly-generated IEPOX-derived SOA. There are two compounds with a fold change > 3 in the control experiments, which includes *m/z* 195

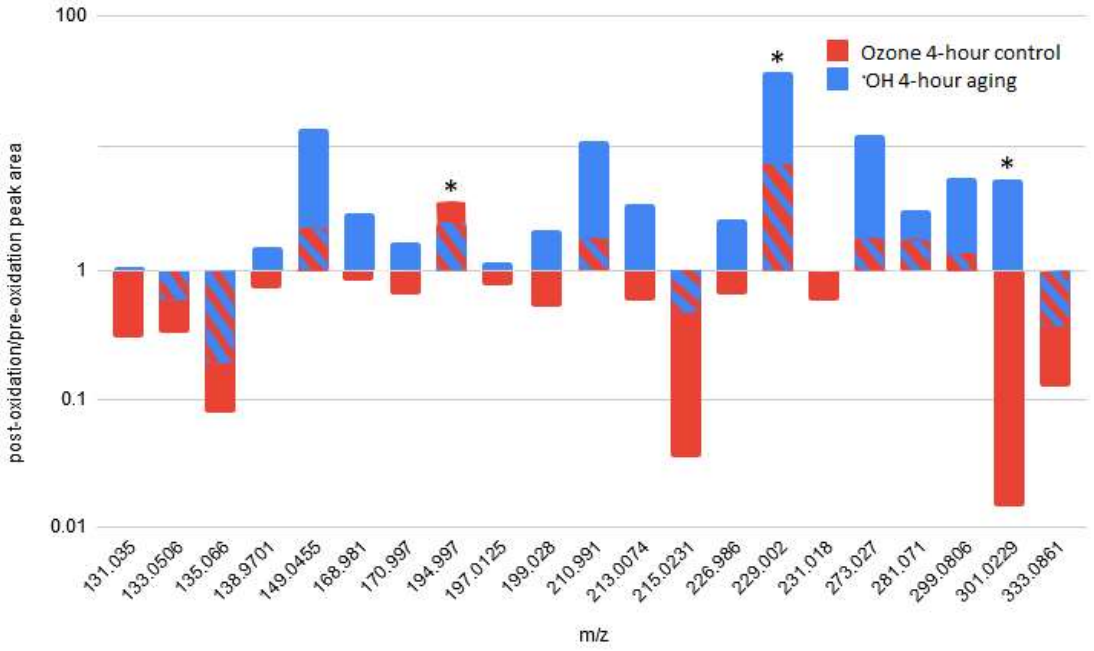

Figure 5. Comparison of geometric mean fold change (EIC peak area from post-oxidation filter/EIC peak area from pre-oxidation filter) for 21 selected $[M–H]^-$ ions from two 4-h control experiments in which freshly-generated IEPOX-derived SOA was aged with O_3 (red) and three 4-h heterogeneous OH oxidation experiments of freshly-generated IEPOX-derived SOA (blue). Color bars are overlaid rather than added to each other, and the striped region represents both red and blue bars. Asterisks denote ions described in the text.

($C_5H_7O_6S^-$) and 229 ($C_5H_9O_8S^-$); there may be other as-yet-uncharacterized reactions or reactions due to contamination causing this. Given that dilution is already corrected for, the large negative fold change of *m/z* 301($C_8H_{13}O_{10}S^-$) may, like *m/z* 333 ($C_{10}H_{21}O_{10}S^-$), be attributed to its status as an early-generation self-reaction product that is consumed during the oxidative aging period, perhaps by compounds that would take part in competing reactions if more oxidant were available.

IEPOX/2-MTS comparison. 4-h oxidative aging experiments were done with either freshly-generated IEPOX-derived SOA or particulate 2-MTSs in order to determine which, if any SOA products, were not formed from heterogeneous •OH oxidation of 2-MTSs. For the experiments (experiments 9 and 10, Table 1) in which particulate 2-MTSs replaced the freshly-generated IEPOX-derived SOA, there were some SOA constituents found in ambient aerosol and aged IEPOX-derived SOA that did not appear, including *m/z* 149 ($C_5H_9O_5^-$), 281 ($C_{10}H_{17}O_7S^-$), 299 ($C_{10}H_{19}O_8S^-$) and 301 ($C_8H_{13}O_{10}S^-$), which may mean that these compounds do not come from heterogeneous •OH oxidation of 2-MTSs. *M/z* 149 ($C_5H_9O_5^-$) is notably not sulfur-containing and is thought to come from the heterogeneous •OH oxidation of 2-MTs (see Scheme 3).[87]

Figure 6 shows the geometric mean fold change for SOA constituents generated from heterogeneous •OH oxidation experiments of 2-MTSs compared again to the 4-h heterogeneous •OH oxidation experiments of freshly-generated IEPOX-derived SOA oxidation. All compounds with fold changes > 3 were also significantly produced during the heterogeneous •OH oxidation experiments of freshly-generated IEPOX-derived SOA. Both heterogeneous •OH oxidation experiments of 2-MTSs showed a large negative fold change (<0.1) of *m/z* 299 ($C_{10}H_{19}O_8S^-$), which indicates that it is produced fairly quickly by an accretion reaction and then consumed either by heterogeneous OH oxidation or by later-generation aerosol-phase reactions. In contrast, though

pre-oxidation peak areas were equivalent with heterogeneous •OH oxidation experiments of freshly-generated IEPOX-derived SOA and particulate 2-MTSs, additional *m/z* 299 was produced during the heterogeneous oxidative aging of IEPOX-derived SOA.

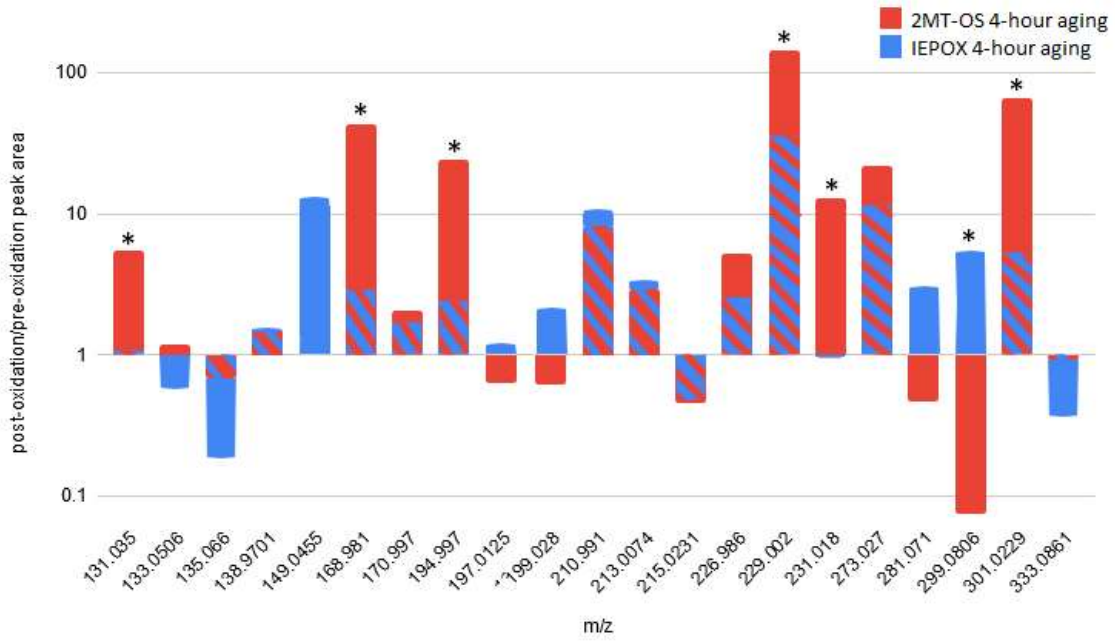

Figure 6. Comparison of geometric mean fold change (EIC peak area from post-oxidation filter/EIC peak area from pre-oxidation filter) for 21 selected $[M–H]^-$ ions from two 4-h heterogeneous OH oxidation experiments of particulate 2-MTSs (red) and three 4-h heterogeneous OH oxidation experiments of freshly-generated IEPOX-derived SOA (blue). Color bars are overlaid rather than added to each other, and the striped region represents both red and blue bars. Asterisks denote ions described the text.

Ions with geometric mean fold change > 3 times greater in the 2-MTS experiments compared to IEPOX-derived SOA experiments include *m/z* 131 ($C_5H_7O_4^-$), 169 ($C_3H_5O_6S^-$), 195 ($C_5H_7O_6S^-$), 229 ($C_5H_9O_8S^-$), 231 ($C_5H_{11}O_8S^-$), and 301 ($C_8H_{13}O_{10}S^-$). In all cases, the 2-MTS aerosols before aging contained smaller amounts of these compounds than did the SOA from IEPOX reactive uptake. The final peak areas for the 2-MTS samples were often, but not always, higher, perhaps attributable to the inclusion of fewer compounds that could further react with them,

acting as sinks. As a note, the total growth of *m/z* 301($C_8H_{13}O_{10}S^-$) during the heterogeneous OH oxidation experiments of particulate 2-MTSs was much smaller than the total growth during the heterogeneous oxidative aging experiments of IEPOX-derived SOA.

Tentative Structural Characterization through MS/MS Analyses. Structures for the tracked compounds are proposed based on MS/MS fragmentation, HILIC retention time, and possible reaction schemes consistent with known isoprene oxidation chemistry[46,59]. For many of the tracked compounds MS/MS analysis was a formality because structures had already been proposed based on the reaction schemes. However, *m/z* 279 ($C_{10}H_{15}O_7S^-$), 281 ($C_{10}H_{17}O_7S^-$), and 283 ($C_{10}H_{19}O_7S^-$), 299 ($C_{10}H_{19}O_8S^-$) and 301 ($C_8H_{13}O_{10}S^-$) do not yet have proposed structures or reaction schemes due in part to insufficient MS/MS data. MS/MS for *m/z* 333 ($C_{10}H_{21}O_{10}S^-$) is included here because although structures were proposed for two isomers by Surratt et al.,[83] the study used RPLC and as such did not achieve good chromatographic separation, which can interfere with single-peak MS/MS.

Fragmentation was assumed to follow standard rules identifying functional groups (e.g.; carboxylic acids are known to lose CO_2 and H_2O), but internal rearrangements are difficult to predict so for simplicity it was assumed that fragmentation was the result of simple cleavage. This presents problems identifying cyclic compounds, although RT allows some insight. Using the HILIC method, less polar compounds elute earlier and more polar compounds later. This can help distinguish between cyclic and non-cyclic isomers with the same formula; for example, when *m/z* 149 ($C_5H_9O_5^-$) is observed to have a retention time of 1.9 min, it must be assumed that this is not the highly polar straight-chain organic acid form but the methyl-tetrahydrofuran form. It can then be assumed that if the organic acid isomer has a place in the reaction pathway (Scheme 3), it is as an intermediate and not as an end product.[59]

Figure 7a shows the EIC for *m/z* 333 ($C_{10}H_{21}O_{10}S^-$, experiment #6), highlighting five major peaks. Four are thought to be diastereomers of the dimer resulting from attack of the 4-hydroxy group of 2-MTS on the tertiary carbon of *trans*-β-IEPOX, and one is thought to be a dimer resulting from attack of the 1-hydroxy group of 2-MTS on the tertiary carbon of *trans*-β-IEPOX. These two structures are shown in Figure 7b. Figure 7c shows a representative MS/MS fragmentation spectrum from the most abundant isomer (RT = 10.29 min). Fragmentation spectra for the other peaks are too similar to determine which might be the isomer resulting from 1-OH attack of 2-MTS, or to differentiate the diastereomers of the 4-OH isomer.

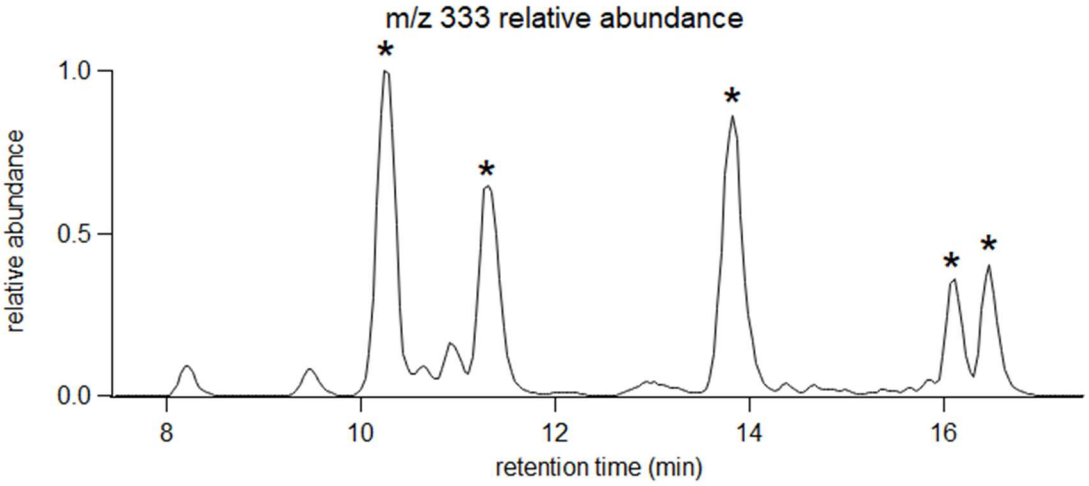

Figure 7a. Relative abundance of $[M–H]^-$ ion detected at *m/z* 333 in post-4-hr-oxidation chamber sample. The five highest peaks, at RTs of 10.29, 11.36, 13.82, 16.13, and 16.49 min, are marked with asterisks.

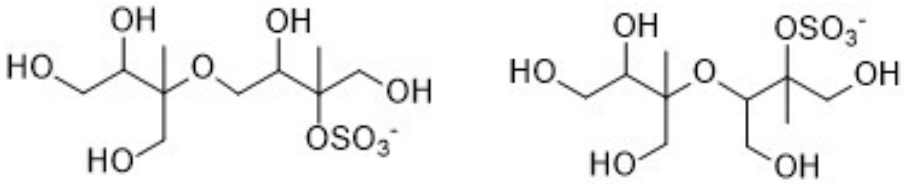

Figure 7b. Structures proposed for the dominant isomers of *m/z* 333. Left: isomer resulting from attack by the 4-OH of 2-MTS. Right: isomer resulting from attack by the 1-OH of 2-MTS.

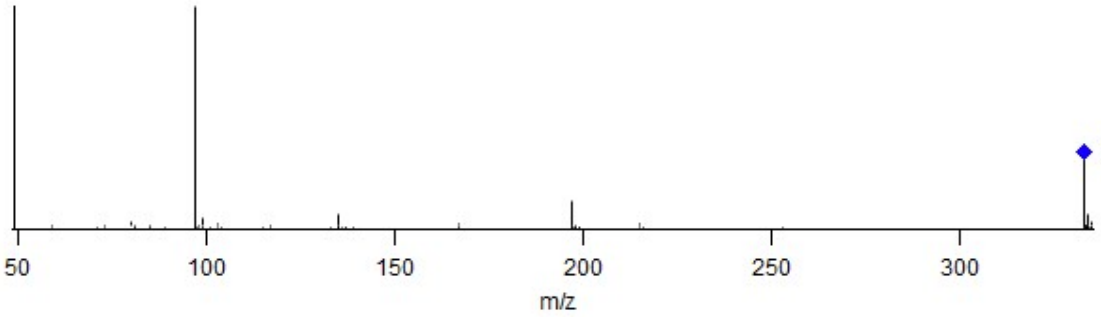

Figure 7c. MS/MS fragmentation spectrum for the highest peak, at RT 10.29 min. The $[M–H]^-$ ion is indicated by a blue diamond.

CHAPTER 4: ATMOSPHERIC RELEVANCE

Compounds tracked in this study were selected predominantly by non-targeted MS analysis and ranked by atmospheric relevance. Selected SOA tracers for heterogeneous •OH oxidation of IEPOX-derived SOA are those found in this study and elsewhere[28,29,88] to have high abundance in atmospheric aerosol from the southeastern United States, the Amazon, and the Galápagos Islands, which are in the low-NO regimes and have $Sulf_{inorg}$ aerosol present. Table 6 shows the 15 most abundant IEPOX-derived SOA constituents (listed as their $[M–H]^-$ ions) in atmospheric $PM_{2.5}$, averaged from the Look Rock TN, Birmingham AL, and Manaus BRA sites, as a fraction of total peak area. Note that these are not compound abundances, because the relative ionization efficiencies of all IEPOX-derived SOA constituents in atmospheric $PM_{2.5}$ have yet to be fully quantified due to lack of availability of authentic standards; with the HILIC/(–)ESI-HR-QTOFMS method, OSs have relatively high ionization efficiency, so they may appear overrepresented here. Other recent studies[18,28] have also found significant amounts of *m/z* 211 and 213 in ambient aerosol, which confirms the relevance of these two compounds, and Hettiyadura et al.[28] found evidence of *m/z* 169, 195, 197, 279, and 281. Other SOA constituents discussed in this study have much lower abundances, though again, for those without a sulfate group (i.e., *m/z* 131 ($C_5H_7O_4^-$), 133 ($C_5H_9O_4^-$), 149 ($C_5H_9O_5^-$), and 151 ($C_5H_{11}O_5^-$)) their true abundance may be higher due to weaker ionization efficiency with the HILIC/(–)ESI-HR-QTOFMS method. It is worth noting that single-particle mass spectrometers, such as the NOAA Particle Analysis Laser Mass Spectrometer (PALMS) and Aerosol Time-of-Flight Mass Spectrometer (ATOFMS), can measure in real-time

2-MTSs (deprotonated ion at *m/z* 215) and the dimer of 2-MTSs (deprotonated ion at *m/z* 333) as well as the 2-MTs (deprotonated ion at *m/z* 135) [25,89]. In addition, these real-time single-particle MS instruments have measured ions at *m/z* 213, 211, 199, 169, 155, 153, and 139 that are attributed to OSs from isoprene oxidation[25,31,89] and identified in the present study and in our recent study as heterogeneous OH oxidation products. Thus, the fact that offline filter analyses by HILIC/ESI-HR-QTOFMS compares so well with these real-time single-particle MS instruments suggests that these SOA constituents are real and not simply filter artifacts.

Table 5. Relative abundance of IEPOX-derived SOA tracer $[M–H]^-$ ions, as EIC peak area/TIC (total ion chromatogram) peak area.

$[M-H]^-$ Ions (*m/z*)	**Relative Abundance**
215.023	17.69%
213.007	1.79%
135.066	1.13%
210.991	1.03%
229.002	0.45%
281.071	0.31%
273.027	0.25%
194.997	0.25%
138.97	0.24%
243.019	0.24%
133.051	0.11%
333.086	0.074%
301.060	0.070%
131.035	0.056%
331.070	0.051%
329.055	0.051%
151.061	0.028%
319.070	0.019%
149.046	0.019%
285.029	0.019%
317.055	0.016%
275.044	0.012%
303.039	0.0095%

Future Work. This study identifies and characterizes some of the most atmospherically abundant IEPOX-derived SOA tracers. Those that are attributed to heterogeneous $^{\bullet}$OH oxidation

represent a sink of fresh IEPOX-derived SOA, and their reaction kinetics are of interest for atmospheric chemistry modelling. With likely structures and formation mechanisms proposed for many of the most atmospherically-abundant IEPOX-derived SOA constituents, including some previously unidentified as being derived from IEPOX, it will become possible to synthesize authentic standards and confirm some of the compounds in chamber mixtures and atmospheric samples. This will also enable quantification, working toward mass closure and branching ratios. The 2-MTs and 2-MTSs make up a large fraction of IEPOX-derived SOA,[25,26,29,51,90] and with the addition of *m/z* 211 and 213, among the most abundant IEPOX-derived OSs in the atmosphere,[28,88,91] it should be possible to find better mass closure for IEPOX-derived SOA. The dimer isomers at *m/z* 333 were not previously identified as being potential precursors in the heterogeneous $^{\bullet}$OH oxidation of freshly-generated IEPOX-derived SOA, and thus, it could be beneficial to synthesize authentic standards for these compounds as well.

To understand the kinetics of heterogeneous $^{\bullet}$OH oxidation, it will be crucial to investigate further the core-shell morphology produced by IEPOX reactive uptake, including how it evolves over time—a time-dependent uptake and mixing coefficient—and under what conditions it forms (e.g. by atomizing aqueous 2-MTSs versus only by IEPOX reactive uptake). Which components of the mixture, or what average OS_C, are critical to form this shell? It could be fruitful to explore real-time single-particle MS methods, such as those used by Hatch et al.[89], or other methods that provide greater time resolution, such as coupling a particle-into-liquid sampler (PILS) with HILIC/ESI-HR-QTOFMS.

Several studies[92,93] have found that isoprene-derived SOA freshly generated without the presence of acidic sulfate is among the least efficient classes of biogenic SOA for ice nucleation, but another recent study found that particles with glassy phase states such as IEPOX-derived SOA

may enhance ice cloud formation[94,95]. Because average O:C (more oxidized molecules) increases during heterogeneous •OH oxidation, and higher O:C has been connected with higher hygroscopicity and more efficient ice nucleation,[96] further investigations may be warranted into whether •OH-aged isoprene-derived SOA has different ice nucleation characteristics. This could be paired with a more concentrated investigation into the ice nucleation or other characteristics of atmospheric SOA. The present study only considered three sampling sites, and could be extended to confirm its relevance at other field sites.

REFERENCES

1. Jimenez, J.L.; Canagaratna, M.R.; Donahue, N.M.; Prevot, A.S.H.; Zhang, Q.; Kroll, J.H.; DeCarlo, P.F.; Allan, J.D.; Coe, H.; Ng, N.L.; Aiken, A.C et al. Evolution of organic aerosols in the atmosphere. *Science* **2009**, *326*(5959), 1525-1529. DOI: 10.1126/science.1180353

2. Guenther, A.B.; Jiang, X.; Heald, C.L.; Sakulyanontvittaya, T.; Duhl, T.; Emmons, L.K.; Wang, X. The Model of Emissions of Gases and Aerosols from Nature version 2.1 (MEGAN2. 1), an extended and updated framework for modeling biogenic emissions. *Geosci. Model Dev.* **2012**, *5*(6), 1471-1471. DOI: 10.5194/gmd-5-1471-2012.

3. Hu, D.; Bian, Q.; Li, T.W.; Lau, A.K.; Yu, J.Z. Contributions of isoprene, monoterpenes, β-caryophyllene, and toluene to secondary organic aerosols in Hong Kong during the summer of 2006. *J. Geophys. Res.* **2008**, *113*(D22). DOI: 10.1029/2008JD010437.

4. Kleindienst, T.E.; Lewandowski, M.; Offenberg, J.H.; Edney, E.O.; Jaoui, M.; Zheng, M.; Ding, X.; Edgerton, E.S. Contribution of primary and secondary sources to organic aerosol and PM2. 5 at SEARCH network sites. *J. Air & Waste Management Assoc.* **2010**, *60*(11), 1388-1399. DOI:10.3155/1047-3289.60.11.1388.

5. Feng, J.; Li, M.; Zhang, P.; Gong, S.; Zhong, M.; Wu, M.; Zheng, M.; Chen, C.; Wang, H.; Lou, S. Investigation of the sources and seasonal variations of secondary organic aerosols in $PM_{2.5}$ in Shanghai with organic tracers. *Atmos. Environ.* **2013**, *79*: 614-622. DOI: 10.1016/j.atmosenv.2013.07.022.

6. Ying, Q.; Li, J.; Kota, S.H. Significant contributions of isoprene to summertime secondary organic aerosol in eastern United States. *Environ. Sci Technol.* **2015**, *49* (13) 7834-7842. DOI: 10.1021/acs.est.5b02514.

7. Surratt, J.D.; Murphy, S.M.; Kroll, J.H.; Ng, N.L.; Hildebrandt, L.; Sorooshian, A.; Szmigielski, R.; Vermeylen, R.; Maenhaut, W.; Claeys, M.; Flagan, R.C. Chemical composition of secondary organic aerosol formed from the photooxidation of isoprene. *J. Phys. Chem. A* **2006**, *110*(31), 9665-9690. DOI: 10.1021/jp061734m.

8. Paulot, F.; Crounse, J.D.; Kjaergaard, H.G.; Kürten, A.; Clair, J.M.S.; Seinfeld, J.H.; Wennberg, P.O. Unexpected epoxide formation in the gas-phase photooxidation of isoprene. *Science* **2009**, *325*(5941), 730-733. DOI: 10.1126/science.1172910.

9. Surratt, J.D.; Chan, A.W.; Eddingsaas, N.C.; Chan, M.; Loza, C.L.; Kwan, A.J.; Hersey, S.P.; Flagan, R.C.; Wennberg, P.O.; Seinfeld, J.H. Reactive intermediates revealed in secondary organic aerosol formation from isoprene. *Proc. Natl. Acad. Sci.* **2010**, *107*(15), 6640-6645. DOI: 10.1073/pnas.0911114107.

10. Lin, Y.H.; Knipping, E.M.; Edgerton, E.S.; Shaw, S.L.; Surratt, J.D. Investigating the influences of SO2 and NH3 levels on isoprene-derived secondary organic aerosol formation using conditional sampling approaches. *Atmos. Chem. Phys.* **2013**, *13*(16), 8457-8470. DOI: 10.5194/acp-13-8457-2013.

11. Bates, K.H.; Crounse, J.D.; St. Clair, J.M.; Bennett, N.B.; Nguyen, T.B.; Seinfeld, J.H.; Stoltz, B.M.; Wennberg, P.O. Gas phase production and loss of isoprene epoxydiols. *J. Phys. Chem. A* **2014**, *118*(7), 1237-1246. DOI: 10.1021/jp4107958.

12. Gaston, C.J.; Riedel, T.P.; Zhang, Z.; Gold, A.; Surratt, J.D.; Thornton, J.A. Reactive uptake of an isoprene-derived epoxydiol to submicron aerosol particles. *Environ. Sci. Technol.* **2014**, *48*(19), 11178-11186. DOI: 10.1021/es5034266.

13. Riedel, T.P.; Lin, Y.H.; Budisulistiorini, S.H.; Gaston, C.J.; Thornton, J.A.; Zhang, Z.; Vizuete, W.; Gold, A.; Surratt, J.D. Heterogeneous reactions of isoprene-derived epoxides: reaction probabilities and molar secondary organic aerosol yield estimates. *Environ. Sci. Technol. Lett.* **2015**, *2*(2), 38-42. DOI: 10.1021/ez500406f.

14. Zhang, Y.; Chen, Y.; Lambe, A.T.; Olson, N.E.; Lei, Z.; Craig, R.L.; Zhang, Z.; Gold, A.; Onasch, T.B.; Jayne, J.T.; Worsnop, D.R. Effect of the aerosol-phase state on secondary organic aerosol formation from the reactive uptake of isoprene-derived epoxydiols (IEPOX). *Environ. Sci. Technol. Lett.* **2018**, *5*(3), 167-174. DOI: 10.1021/acs.estlett.8b00044.

15. Nguyen, T.B.; Coggon, M.M.; Bates, K.H.; Zhang, X.; Schwantes, R.H.; Schilling, K.A.; Loza, C.L.; Flagan, R.C.; Wennberg, P.O.; Seinfeld, J.H. Organic aerosol formation from the reactive uptake of isoprene epoxydiols (IEPOX) onto non-acidified inorganic seeds. *Atmos. Chem. Phys.* **2014**, *14*(7), 3497-3510. DOI: 10.5194/acp-14-3497-2014.

16. Riva, M.; Chen, Y.; Zhang, Y.; Lei, Z.; Olson, N.E.; Boyer, H.C.; Narayan, S.; Yee, L.D.; Green, H.S.; Cui, T.; Zhang, Z. Increasing Isoprene Epoxydiol-to-Inorganic Sulfate Aerosol Ratio Results in Extensive Conversion of Inorganic Sulfate to Organosulfur Forms: Implications for Aerosol Physicochemical Properties. *Environ. Sci. Technol.* **2019**, *53*(15), 8682-8694. DOI: 10.1021/acs.est.9b01019.

17. Zhang, Y.; Chen, Y.; Lei, Z.; Olson, N.E.; Riva, M.; Koss, A.R.; Zhang, Z.; Gold, A.; Jayne, J.T.; Worsnop, D.R.; Onasch, T.B. Joint Impacts of Acidity and Viscosity on the Formation of Secondary Organic Aerosol from Isoprene Epoxydiols (IEPOX) in Phase Separated Particles. *ACS Earth Space Chem.* **2019**, *3*(12), 2646-2658. DOI: 10.1021/acsearthspacechem.9b00209.

18. Hughes, D.D. and Stone, E.A. Organosulfates in the Midwestern United States: abundance, composition and stability. *Environ. Chem.* **2019**, *16*(5), 312-322. DOI: 10.1071/EN18260.

19. Fulara, J.; Erattupuzha, S.; Garkusha, I.; Maier, J.P. Structure and Electronic Transitions of

$C_7H_4O_2^+$ and $C_7H_5O_2^+$ Ions: Neon Matrix and Theoretical Studies. *J. Phys. Chem. A* **2016**, *120*(51), 10134-10140. DOI: 10.1021/acs.jpca.6b10687.

20. Xu, L.; Guo, H.; Weber, R.J.; Ng, N.L. Chemical characterization of water-soluble organic aerosol in contrasting rural and urban environments in the southeastern United States. *Environ. Sci. Technol.* 2017, 51, 1, 78-88. DOI: 10.1021/acs.est.6b05002.

21. Zhao, Z.; Wang, Y.; Qin, M.; Hu, Y.; Xie, Y.; Russell, A.G. Drought Impacts on Secondary Organic Aerosol: A Case Study in the Southeast United States. *Environ. Sci. Technol.* **2019**, *53*(1), 242-250. DOI: 10.1021/acs.est.8b04842.

22. Riva, M.; Budisulistiorini, S.H.; Chen, Y.; Zhang, Z.; D'Ambro, E.L.; Zhang, X.; Gold, A.; Turpin, B.J.; Thornton, J.A.; Canagaratna, M.R.; Surratt, J.D. Chemical characterization of secondary organic aerosol from oxidation of isoprene hydroxyhydroperoxides. *Environ. Sci. Technol.* **2016**, *50*(18), 9889-9899. DOI: 10.1021/acs.est.6b02511.

23. Isaacman-VanWertz, G.; Yee, L.D.; Kreisberg, N.M.; Wernis, R.; Moss, J.A.; Hering, S.V.; de Sá, S.S.; Martin, S.T.; Alexander, M.L.; Palm, B.B.; Hu, W. Ambient gas-particle partitioning of tracers for biogenic oxidation. *Environ. Sci. Technol.* **2016**, *50*(18), (2016), 9952-9962. DOI: doi.org/10.1021/acs.est.6b01674.

24. Shrivastava, M.; Andreae, M.O.; Artaxo, P.; Barbosa, H.M.; Berg, L.K.; Brito, J.; Ching, J.; Easter, R.C.; Fan, J.; Fast, J.D.; Feng, Z.Urban pollution greatly enhances formation of natural aerosols over the Amazon rainforest. *Nat. Commun.* **2019**, *10*(1), 1-12. DOI: 10.1038/s41467-019-08909-4.

25. Froyd, K.D.; Murphy, S.M.; Murphy, D.M.; De Gouw, J.A.; Eddingsaas, N.C.; Wennberg, P.O. Contribution of isoprene-derived organosulfates to free tropospheric aerosol mass. *Proc. Natl. Acad. Sci.* **2010**, *107*(50), 21360-21365. DOI: 10.1073/pnas.1012561107.

26. Budisulistiorini, S.; Li, X.; Bairai, S.T.; Renfro, J.; Liu, Y.; Liu, Y.J.; McKinney, K.A.; Martin, S.T.; McNeill, V.F.; Pye, H.O.T.; Nenes, A. Examining the effects of anthropogenic emissions on isoprene-derived secondary organic aerosol formation during the 2013 Southern Oxidant and Aerosol Study (SOAS) at the Look Rock, Tennessee ground site. *Atmos. Chem. Phys.* **2015**, 15: 8871-8888. DOI: 10.5194/acp-15-8871-2015.

27. Zhang, Y.; Nichman, L.; Spencer, P.; Jung, J.I.; Lee, A.; Heffernan, B.K.; Gold, A.; Zhang, Z.; Chen, Y.; Canagaratna, M.R; Jayne, J.T. The Cooling Rate-and Volatility-Dependent Glass-Forming Properties of Organic Aerosols Measured by Broadband Dielectric Spectroscopy. *Environ. Sci. Technol.* **2019**, *53*(21), 12366-12378. DOI: 10.1021/acs.est.9b03317.

28. Hettiyadura, A.P.S.; Al-Naiema, I.M.; Hughes, D.D.; Fang, T.; Stone, E.A. Organosulfates in Atlanta, Georgia: anthropogenic influences on biogenic secondary organic aerosol formation.

Atmos. Chem. Phys. **2019**, *19*(5), 3191-3206. DOI: 10.5194/acp-19-3191-2019.

29. Cui, T.; Zeng, Z.; dos Santos, E.O.; Zhang, Z.; Chen, Y.; Zhang, Y.; Rose, C.A.; Budisulistiorini, S.H.; Collins, L.B.; Bodnar, W.M.; de Souza, R.A. Development of a hydrophilic interaction liquid chromatography (HILIC) method for the chemical characterization of water-soluble isoprene epoxydiol (IEPOX)-derived secondary organic aerosol. *Environ. Sci. Processes & Impacts* **2018**, *20*(11), 1524-1536. DOI: 10.1039/C8EM00308D.

30. Froyd, K.D.; Murphy, D.M.; Lawson, P.; Baumgardner, D.; Herman, R.L. Aerosols that form subvisible cirrus at the tropical tropopause. *Atmos. Chem. Phys.* **2010**, *10*(1), 209-218. atmos-chem-phys.net/10/209/2010.

31. Liao, J.; Froyd, K.D.; Murphy, D.M.; Keutsch, F.N.; Yu, G.; Wennberg, P.O.; Clair, J.M.S.; Crounse, J.D.; Wisthaler, A.; Mikoviny, T.; Jimenez, J.L. Airborne measurements of organosulfates over the continental US. *J. Geophys. Res.* **2015**, *120*(7), 2990-3005. DOI: 10.1002/2014JD022378.

32. Pratt, K.A.; Fiddler, M.N.; Shepson, P.B.; Carlton, A.G.; Surratt, J.D. Organosulfates in cloud water above the Ozarks' isoprene source region. *Atmos. Environ.* **2013**, *77*: 231-238. DOI: 10.1016/j.atmosenv.2013.05.011.

33. Boone, E.J.; Laskin, A.; Laskin, J.; Wirth, C.; Shepson, P.B.; Stirm, B.H.; Pratt, K.A. Aqueous processing of atmospheric organic particles in cloud water collected via aircraft sampling. *Environ. Sci. Technol.* **2015**, *49*(14), 8523-8530. DOI: 10.1021/acs.est.5b01639.

34. Spolnik, G.; Wach, P.; Rudziński, K.J.; Szmigielski, R.; Danikiewicz, W. Tracing the biogenic secondary organic aerosol markers in rain, snow and hail. *Chemosphere* **2020**, *251*: 126439. DOI: 10.1016/j.chemosphere.2020.126439.

35. Pye, H.O.T.; Pinder, R.W.; Piletic, I.R.; Xie, Y.; Capps, S.L.; Lin, Y.H.; Surratt, J.D.; Zhang, Z.; Gold, A.; Luecken, D.J.; Hutzell, W.T. Epoxide pathways improve model predictions of isoprene markers and reveal key role of acidity in aerosol formation. *Environ. Sci. Technol.* **2013**, *47*(19), 11056-11064. DOI: 10.1021/es402106h.

36. McNeill, V.F. Aqueous organic chemistry in the atmosphere: Sources and chemical processing of organic aerosols. *Environ. Sci. Technol.* **2015**, *49*(3), 1237-1244. DOI: 10.1021/es5043707.

37. Surratt, J.D.; Lin, Y.H.; Arashiro, M.; Vizuete, W.G.; Zhang, Z.; Gold, A.; Jaspers, I.; Fry, R.C. Understanding the Early Biological Effects of Isoprene-Derived Particulate Matter Enhanced by Anthropogenic Pollutants. *Research report (Health Eff. Inst.)* **2019**, (*198*), p.1.

38. Kramer, A.J.; Rattanavaraha, W.; Zhang, Z.; Gold, A.; Surratt, J.D.; Lin, Y.H. Assessing the

oxidative potential of isoprene-derived epoxides and secondary organic aerosol. *Atmos. Environ.* **2016**, *130*: 211-218. DOI: 10.1016/j.atmosenv.2015.10.018.

39. Tuet, W.Y.; Chen, Y.; Fok, S.; Champion, J.A.; Ng, N.L. Inflammatory responses to secondary organic aerosols (SOA) generated from biogenic and anthropogenic precursors. *Atmos. Chem. Phys.* **2017**, *17*(18), 11423. DOI: 10.5194/acp-17-11423-2017.

40. Rattanavaraha, W.; Rosen, E.; Zhang, H.; Li, Q.; Pantong K.; Kamens, R.M. The reactive oxidant potential of different types of aged atmospheric particles: An outdoor chamber study. *Atmos. Environ.*, **2011**, *45*(23), 3848-3855. DOI: j.atmosenv.2011.04.002.

41. Lin, Y.H.; Arashiro, M.; Martin, E.; Chen, Y.; Zhang, Z.; Sexton, K.G.; Gold, A.; Jaspers, I.; Fry, R.C.; Surratt, J.D. Isoprene-derived secondary organic aerosol induces the expression of oxidative stress response genes in human lung cells. *Environ. Sci. Technol. Lett.* **2016**, *3*(6), 250-254. DOI: 10.1021/acs.estlett.6b00151.

42. St. Clair, J.M.; Rivera-Rios, J.C.; Crounse, J.D.; Knap, H.C.; Bates, K.H.; Teng, A.P.; Jørgensen, S.; Kjaergaard, H.G.; Keutsch, F.N.; Wennberg, P.O. Kinetics and products of the reaction of the first-generation isoprene hydroxy hydroperoxide (ISOPOOH) with OH. *J. Phys. Chem. A.* **2016**, *120*(9), 1441-1451. DOI: 10.1021/acs.jpca.5b06532.

43. Krechmer, J.E.; Coggon, M.M.; Massoli, P.; Nguyen, T.B.; Crounse, J.D.; Hu, W.; Day, D.A.; Tyndall, G.S.; Henze, D.K.; Rivera-Rios, J.C.; Nowak, J.B. Formation of low volatility organic compounds and secondary organic aerosol from isoprene hydroxyhydroperoxide low-NO oxidation. *Environ. Sci. Technol.* **2015**, *49*(17), 10330-10339. DOI: 10.1021/acs.est.5b02031.

44. Liu, J.; D'Ambro, E.L.; Lee, B.H.; Lopez-Hilfiker, F.D.; Zaveri, R.A.; Rivera-Rios, J.C.; Keutsch, F.N.; Iyer, S.; Kurten, T.; Zhang, Z.; Gold, A. Efficient isoprene secondary organic aerosol formation from a non-IEPOX pathway. *Environ. Sci. Technol.* **2016**, *50*(18), 9872-9880. DOI: 10.1021/acs.est.6b01872.

45. D'Ambro, E.L.; Lee, B.H.; Liu, J.; Shilling, J.E.; Gaston, C.J.; Lopez-Hilfiker, F.D.; Schobesberger, S.; Zaveri, R.A.; Mohr, C.; Lutz, A.; Zhang, Z. Molecular composition and volatility of isoprene photochemical oxidation secondary organic aerosol under low-and high-NO_x conditions. *Atmos. Chem. Phys.* **2017**, *17*(1), 159-174. DOI: 10.5194/acp-17-159-2017.

46. Lam, H.K.; Kwong, K.C.; Poon, H.Y.; Davies, J.F.; Zhang, Z.; Gold, A.; Surratt, J.D.; Chan, M.N. Heterogeneous OH oxidation of isoprene-epoxydiol-derived organosulfates: kinetics, chemistry and formation of inorganic sulfate. *Atmos. Chem. Phys.* **2019**, *19*(4), 2433-2440. DOI: 10.5194/acp-19-2433-2019.

47. Wach, P.; Spolnik, G.; Surratt, J.D.; Blaziak, K.; Rudzinski, K.; Lin, Y.H.; Maenhaut, W.; Danikiewicz, W.; Claeys, M.; Szmigielski, R. Structural characterization of lactone-containing

MW 212 organosulfates originating from isoprene oxidation in ambient fine aerosol. *Environ. Sci. Technol.* **2020**, 54(3), 1415-1424. DOI: 10.1021/acs.est.9b06190.

48. Gómez-González, Y.; Surratt, J.D.; Cuyckens, F.; Szmigielski, R.; Vermeylen, R.; Jaoui, M.; Lewandowski, M.; Offenberg, J.H.; Kleindienst, T.E.; Edney, E.O.; Blockhuys, F. Characterization of organosulfates from the photooxidation of isoprene and unsaturated fatty acids in ambient aerosol using liquid chromatography/(−) electrospray ionization mass spectrometry. *J. Mass Spec.* **2008**, *43*(3), 371-382. DOI: doi.org/10.1002/jms.1329.

49. Surratt, J.D.; Gómez-González, Y.; Chan, A.W.; Vermeylen, R.; Shahgholi, M.; Kleindienst, T.E.; Edney, E.O.; Offenberg, J.H.; Lewandowski, M.; Jaoui, M.; Maenhaut, W. Organosulfate formation in biogenic secondary organic aerosol. *J. Phys. Chem. A* **2008**, *112*(36), 8345-8378. DOI: 10.1021/jp802310p.

50. Kristensen, K. and Glasius, M. Organosulfates and oxidation products from biogenic hydrocarbons in fine aerosols from a forest in North West Europe during spring. *Atmos. Environ.* **2001**, *45*(27), 4546-4556. DOI: 10.1016/j.atmosenv.2011.05.063.

51. Lin, Y.H.; Knipping, E.M.; Edgerton, E.S.; Shaw, S.L.; Surratt, J.D. Investigating the influences of SO_2 and NH_3 levels on isoprene-derived secondary organic aerosol formation using conditional sampling approaches. *Atmos. Chem. Phys.* **2013**, *13*(16), 8457-8470. DOI: 10.5194/acp-13-8457-2013.

52. Brüggemann, M.; Poulain, L.; Held, A.; Stelzer, T.; Zuth, C.; Richters, S.; Mutzel, A.; van Pinxteren, D.; Iinuma, Y.; Katkevica, S. and Rabe, R. Real-time detection of highly oxidized organosulfates and BSOA marker compounds during the F-BEACh 2014 field study. *Atmos. Chem. Phys.* **2017**, *17*(2), 1453-1469. DOI: 10.5194/acp-17-1453-2017.

53. Claeys, M.; Graham, B.; Vas, G.; Wang, W.; Vermeylen, R.; Pashynska, V.; Cafmeyer, J.; Guyon, P.; Andreae, M. O.; Artaxo, P.; Maenhaut, W. Formation of secondary organic aerosols through photooxidation of isoprene. *Science* **2004**, *303*(5661), 1173−1176. DOI: 10.1016/j.atmosenv.2004.06.001.

54. Zhang, H.; Zhang, Z.; Cui, T.; Lin, Y.H.; Bhathela, N.A.; Ortega, J.; Worton, D.R.; Goldstein, A.H.; Guenther, A.; Jimenez, J.L.; Gold, A. Secondary organic aerosol formation via 2-methyl-3-buten-2-ol photooxidation: Evidence of acid-catalyzed reactive uptake of epoxides. *Environ. Sci. Technol. Lett.* **2014**, *1*(4), 242-247. DOI: 10.1021/ez500055f.

55. Ganzeveld, L. & Lelieveld, J. Impact of Amazonian deforestation on atmospheric chemistry. *Geophys. Res. Lett.* **2004**, *31*(6). DOI: 10.1029/2003GL019205.

56. Arneth, A.; Harrison, S.P.; Zaehle, S.; Tsigaridis, K.; Menon, S.; Bartlein, P.J.; Feichter, J.; Korhola, A.; Kulmala, M.; O'Donnell, D.; Schurgers, G. Terrestrial biogeochemical feedbacks

in the climate system. *Nature Geosci.* **2010**, *3*(8), 525-532.

57. Pöschl, U.; Martin, S.T.; Sinha, B.; Chen, Q.; Gunthe, S.S.; Huffman, J.A.; Borrmann, S.; Farmer, D.K.; Garland, R.M.; Helas, G.; Jimenez, J.L. Rainforest aerosols as biogenic nuclei of clouds and precipitation in the Amazon. *Science* **2010**, *329*(5998), 1513-1516. DOI: 10.1126/science.1191056.

58. Hu, W.; Palm, B.B.; Day, D.A.; Campuzano-Jost, P.; Krechmer, J.E.; Peng, Z.; de Sá, S.S.; Martin, S.T.; Koss, A.; de Gouw, J.A.; Jimenez, J.L. Volatility and lifetime against OH heterogeneous reaction of ambient isoprene-epoxydiols-derived secondary organic aerosol (IEPOX-SOA). *Atmos. Chem. Phys.* **2016**, *16*(18). DOI: 10.5194/acp-16-11563-2016.

59. Chen, Y.; Zhang, Y.; Lambe, A.T.; Xu, R.; Lei, Z.; Olson, N. E.; Zhang, Z.; Szalkowski, T.; Cui, T.; Vizuete, W.; Gold, A.; Turpin, B.J.; Ault, A.P.; Chan, M.N.; Surratt, J. D. Heterogeneous hydroxyl radical oxidation of isoprene-epoxydiol-derived methyltetrol sulfates: plausible formation mechanisms of previously unexplained organosulfates in ambient fine aerosols. *Environ. Sci. Technol. Lett.* **2020**, https://doi.org/10.1021/acs.estlett.0c00276.

60. Prinn, R.; Huang, J.; Weiss, R.; Cunnold, D.; Fraser, P.; Simmonds, P.; McCulloch, A.; Harth, C.; Salameh, P.; O'Doherty, S.; Wang,R.; Porter, L.; Miller, B. Evidence for substantial variations of atmospheric hydroxyl radicals in the past two decades. *Science* **2001**, *292*, 1882-1888.

61. You, Y.; Renbaum-Wolff, L.; Carreras-Sospedra, M.; Hanna, S.J.; Hiranuma, N.; Kamal, S.; Smith, M. L.; Zhang, X.; Weber, R. J.; Shilling, J. E.; Dabdub, D.; Martin, S. T.; Bertram, A. K. Images reveal that atmospheric particles can undergo liquid−liquid phase separations. *Proc. Natl. Acad. Sci.* **2012**, *109*(33), 13188−13193. DOI: 10.1073/pnas.1206414109.

62. Smith, M. L.; You, Y.; Kuwata, M.; Bertram, A. K.; Martin, S. T. Phase Transitions and Phase Miscibility of Mixed Particles of Ammonium Sulfate, Toluene-Derived Secondary Organic Material, and Water. *J. Phys. Chem. A* **2013**, *117*(36), 8895−8906. DOI: 10.1021/jp405095e.

63. Ryder, O. S.; Ault, A. P.; Cahill, J. F.; Guasco, T. L.; Riedel, T.P.; Cuadra-Rodriguez, L. A.; Gaston, C. J.; Fitzgerald, E.; Lee, C.; Prather, K. A.; Bertram, T. H. On the Role of Particle Inorganic Mixing State in the Reactive Uptake of N_2O_5 to Ambient Aerosol Particles. *Environ. Sci. Technol.* **2014**, *48*(3), 1618−1627. DOI: 10.1021/es4042622.

64. O'Brien, R. E.; Wang, B.; Kelly, S. T.; Lundt, N.; You, Y.; Bertram, A. K.; Leone, S. R.; Laskin, A.; Gilles, M. K. Liquid−Liquid Phase Separation in Aerosol Particles: Imaging at the Nanometer Scale. *Environ. Sci. Technol.* **2015**, *49*(8), 4995−5002. DOI: 10.1021/acs.est.5b00062.

65. Renbaum-Wolff, L.; Song, M.; Marcolli, C.; Zhang, Y.; Liu, P. F.; Grayson, J. W.; Geiger, F.

M.; Martin, S. T.; Bertram, A. K. Observations and implications of liquid−liquid phase separation at high relative humidities in secondary organic material produced by α-pinene ozonolysis without inorganic salts. *Atmos. Chem. Phys.* **2016**, *16*(12), 7969−7979. DOI: 10.5194/acp-16-7969-2016.

66. Ault, A. P.; Axson, J. L. Atmospheric Aerosol Chemistry: Spectroscopic and Microscopic Advances. *Anal. Chem.* **2017**, *89*(1), 430−452. DOI: 10.1021/acs.analchem.6b04670.

67. Jacobs, M.I.; Darer, A.I. and Elrod, M.J.. Rate constants and products of the OH reaction with isoprene-derived epoxides. *Environ. Sci. Technol.* **2013**, *47*(22), 12868-12876. DOI: 10.1021/es403340g.

68. Zhang, Z.; Lin, Y.H.; Surratt, J.D.; Ball, L.M.; Gold, A. Technical Note: Synthesis of isoprene atmospheric oxidation products: isomeric epoxydiols and the rearrangement products cis-and trans-3-methyl-3, 4-dihydroxytetrahydrofuran. *Atmos. Chem. Phys. Discussions* **2012**, *12*(6) 8529-8535.

69. Lambe, A.T.; Zhang, J.; Sage, A.M. and Donahue, N.M. Controlled OH radical production via ozone-alkene reactions for use in aerosol aging studies. *Environ. Sci. Technol.* **2007**, 41(7), 2357-2363. DOI: 10.1021/es061878e.

70. Ribeiro, I.O.; do Santos, E.O.; Batista, C.E.; Fernandes, K.S.; Ye, J.; Medeiros, A.S.; e Oliveira, R.L.; de Sá, S.S.; de Sousa, T.R.; Kayano, M.T.; Andreoli, R.V. Impact of biomass burning on a metropolitan area in the Amazon during the 2015 El Niño: The enhancement of carbon monoxide and levoglucosan concentrations. *Environ. Pollution* **2020**, *260*, p.114029. DOI: 10.1016/j.envpol.2020.114029.

71. Kristiansen, N. I.; Stohl, A.; Olivi., D. J. L.; Croft, B.; S.vde, O. A.; Klein, H.; Christoudias, T.; Kunkel, D.; Leadbetter, S. J.; Lee, Y. H.; Zhang, K.; Tsigaridis, K.; Bergman, T.; Evangeliou, N.; Wang, H.; Ma, P.-L.; Easter, R. C.; Rasch, P. J.; Liu, X.; Pitari, G.; Genova, G. D.; Zhao, S. Y.; Balkanski, Y.; Bauer, S. E.; Faluvegi, G. S.; Kokkola, H.; Martin, R. V.; Pierce, J. R.; Schulz, M.; Shindell, D.; Tost, H.; Zhang, H. Evaluation of Observed and Modelled Aerosol Lifetimes Using Radioactive Tracers of Opportunity and an Ensemble of 19 Global Models. *Atmos. Chem. Phys.* **2016**, *16*(5), 3525–3561. DOI: 10.5194/acp-16-3525-2016.

72. Bryant, D. J.; Dixon, W. J.; Hopkins, J. R.; Dunmore, R. E.; Pereira, K. L.; Shaw, M.; Squires, F. A.; Bannan, T. J.; Mehra, A.; Worrall, S. D.; Bacak, A.; Coe, H.; Percival, C. J.; Whalley, L. K.; Heard, D. E.; Slater, E. J.; Ouyang, B.; Cui, T.; Surratt, J. D.; Liu, D.; Shi, Z.; Harrison, R.; Sun, Y.; Xu, W.; Lewis, A. C.; Lee, J. D.; Rickard, A. R.; Hamilton, J. F. Strong Anthropogenic Control of Secondary Organic Aerosol Formation from Isoprene in Beijing. *Atmos. Chem. Phys. Discuss.* **2019**, 1–30. DOI: 10.5194/acp-2019-929.

73. Russell, G. A. Deuterium-Isotope Effects in the Autoxidation of Aralkyl Hydrocarbons. Mechanism of the Interaction of Peroxy Radicals *J. Am. Chem. Soc.* **1957**, *79* (14), 3871–3877. DOI: 10.1021/ja01571a068.

74. Bennett, J. E.; Summers, R. Product Studies of the Mutual Termination Reactions of Sec-Alkylperoxy Radicals: Evidence for Non-Cyclic Termination. *Can. J. Chem.* **1974**, *52*(8), 1377–1379. DOI: 10.1139/v74-209.

75. Suárez, E. and Rodriguez, M.S. β-Fragmentation of Alkoxyl Radicals: Synthetic Applications. *Radicals in Organic Syntheses* **2001**, chapter 5.3, pp.440-454.

76. Salamone, M.; Bietti, M. Reaction Pathways of Alkoxyl Radicals. The Role of Solvent Effects on C–C Bond Fragmentation and Hydrogen Atom Transfer Reactions. *Synlett* **2014**, *25*(13), 1803–1816. DOI: 10.1055/s-0033-1341280.

77. Bothe, E.; Schuchmann, M. N.; Schulte-Frohlinde, D.; Sonntag, C. von. HO_2 Elimination from α-hydroxyalkylperoxy radicals in aqueous solution. *Photochem. Photobiol.* **1978**, *28*(4–5), 639–643. DOI: 10.1111/j.1751-1097.1978.tb06984.x.

78. Bothe, E.; Schulte-Frohlinde, D.; Sonntag, C. von. Radiation Chemistry of Carbohydrates. Part 16. Kinetics of HO2? Elimination from Peroxyl Radicals Derived from Glucose and Polyhydric Alcohols. *J. Chem. Soc. Perkin Transactions 2* **1978**, *0*(5), 416. DOI: 10.1039/p29780000416.

79. Fischer, E.; Speier, A. Darstellung Der Ester. *Ber. Dtsch. Chem. Ges.* **1895**, *28*(3), 3252–3258. DOI: 10.1002/cber.189502803176.

80. Zimmermann, H.; Rudolph, J. Protonic States and the Mechanism of Acid-Catalysed Esterification. *Angewandte Chemie Int. Ed. Engl.* **1965**, *4*(1), 40–49. DOI: 10.1002/anie.196500401.

81. Ziemann, P. J.; Atkinson, R. Kinetics, Products, and Mechanisms of Secondary Organic Aerosol Formation. *Chem. Soc. Rev.* **2012**, *41*(19), 6582–6605. DOI: 10.1039/c2cs35122f.

82. Adickes, H. W.; Politzer, I. R.; Meyers, A. I. Aldehydes from Dihydro-1,3-Oxazines. Synthesis of Gamma-Hydroxy Aldehydes and Their Gamma-Oxo Derivatives. *J. Am. Chem. Soc.* **1969**, *91*(8), 2155–2156. DOI: 10.1021/ja01036a076.

83. Surratt, J.D.; Gómez-González, Y.; Chan, A.W.; Vermeylen, R.; Shahgholi, M.; Kleindienst, T.E.; Edney, E.O.; Offenberg, J.H.; Lewandowski, M.; Jaoui, M.; Maenhaut, W. Organosulfate formation in biogenic secondary organic aerosol. *J. Phys. Chem. A* **2008**, *112*(36), pp.8345-8378. DOI: 10.1021/jp802310p.

84. Darer, A.I.; Cole-Filipiak, N.C.; O'Connor, A.E.; Elrod, M.J. Formation and stability of atmospherically relevant isoprene-derived organosulfates and organonitrates. *Environ. Sci. Technol.* **2011**, *45*(5), pp.1895-1902. DOI: 10.1021/es103797z.

85. Hu, K.S.; Darer, A.I.; Elrod, M.J. Thermodynamics and kinetics of the hydrolysis of atmospherically relevant organonitrates and organosulfates. *Atmos. Chem. Phys.* **2011**, *11*(16). DOI: 10.5194/acp-11-8307-2011.

86. Ervens, B. Modeling the processing of aerosol and trace gases in clouds and fogs. *Chem. Rev.* **2015**, *115*(10), pp.4157-4198. DOI: 10.1021/cr5005887.

87. Jaoui, M.; Szmigielski, R.; Nestorowicz, K.; Kolodziejczyk, A.; Sarang, K.; Rudzinski, K.J.; Konopka, A.; Bulska, E.; Lewandowski, M.; Kleindienst, T.E. Organic Hydroxy Acids as Highly Oxygenated Molecular (HOM) Tracers for Aged Isoprene Aerosol. *Environ. Sci. Technol.* **2019**, *53*(24), pp.14516-14527. DOI: 10.1021/acs.est.9b05075.

88. Hettiyadura, A.P.; Jayarathne, T.; Baumann, K.; Goldstein, A.H.; de Gouw, J.A.; Koss, A.,; Keutsch, F.N.; Skog, K.; Stone, E.A. Qualitative and quantitative analysis of atmospheric organosulfates in Centreville, Alabama. *Atmos. Chem. Phys.* **2017**, *17*, 1343–1359. DOI: 10.5194/acp-17-1343-2017.

89. Hatch, L.E.; Creamean, J.M.; Ault, A.P.; Surratt, J.D.; Chan, M.N.; Seinfeld, J.H.; Edgerton, E.S.; Su, Y.; Prather, K.A. Measurements of isoprene-derived organosulfates in ambient aerosols by aerosol time-of-flight mass spectrometry-Part 1: Single particle atmospheric observations in Atlanta. *Environ. Sci. Technol.* **2011**, *45*(12), pp.5105-5111. DOI: 10.1021/es103944a.

90. Hu, W.W.; Campuzano-Jost, P.; Palm, B.; Day, D.A.; Ortega, A.; Hayes, P.; Krechmer, J.; Chen, Q.; Kuwata, M.; Liu, Y.; de Sá, S. Characterization of a real-time tracer for isoprene epoxydiols-derived secondary organic aerosol (IEPOX-SOA) from aerosol mass spectrometer measurements. *Atmos. Chem. Phys., Eur. Geosci. Union* **2015**, *15*(20), pp.11807-11833. DOI: 10.5194/acp-15-11807-2015.

91. Hettiyadura, A.P.S.; Stone, E.A.; Kundu, S.; Baker, Z.; Geddes, E.; Richards, K.; Humphry, T. Determination of atmospheric organosulfates using HILIC chromatography with MS detection. *Atmos. Meas. Techniques*, **2015**, *8*(6). DOI: 10.5194/amt-8-2347-2015.

92. Berkemeier, T.; Shiraiwa, M.; Pöschl, U.; Koop, T. Competition between water uptake and ice nucleation by glassy organic aerosol particles. *Atmos. Chem. Phys.* **2014**, *14*(22). DOI: 10.5194/acp-14-12513-2014.

93. Charnawskas, J.C.; Alpert, P.A.; Lambe, A.T.; Berkemeier, T.; O'Brien, R.E.; Massoli, P.; Onasch, T.B.; Shiraiwa, M.; Moffet, R.C.; Gilles, M.K.; Davidovits, P. Condensed-phase

biogenic–anthropogenic interactions with implications for cold cloud formation. *Faraday discussions* **2017**, *200*, 165-194. DOI: 10.1039/c7fd00010c.

94. Zhang, Y.; Nichman, L.; Spencer, P.; Jung, J.I.; Lee, A.; Heffernan, B.K.; Gold, A.; Zhang, Z.; Chen, Y.; Canagaratna, M.R.; Jayne, J.T.. The Cooling Rate-and Volatility-Dependent Glass-Forming Properties of Organic Aerosols Measured by Broadband Dielectric Spectroscopy. *Environ. Sci. Technol.* **2019**, *53*(21), pp.12366-12378.

95. Murray, B. J.; Wilson, T. W.; Dobbie, S.; Cui, Z.; Al-Jumur, S. M. R. K.; Möhler, O.; Schnaiter, M.; Wagner, R.; Benz, S.; Niemand, M.; Saathoff, H.; Ebert, V.; Wagner, S.; Kärcher, B. Heterogeneous nucleation of ice particles on glassy aerosols under cirrus conditions. *Nat. Geosci*. Zhang, Y., Nichman, L., Spencer, P., Jung, J.I., Lee, A., Heffernan, B.K., Gold, A., Zhang, Z., Chen, Y., Canagaratna, M.R. and Jayne, J.T., 2019. The Cooling Rate-and Volatility-Dependent Glass-Forming Properties of Organic Aerosols Measured by Broadband Dielectric Spectroscopy. *Environ. Sci. Technol.* **2019**, *53*(21), pp.12366-12378.

96. Wang, B.; Lambe, A.T.; Massoli, P.; Onasch, T.B.; Davidovits, P.; Worsnop, D.R.; Knopf, D.A. The deposition ice nucleation and immersion freezing potential of amorphous secondary organic aerosol: Pathways for ice and mixed-phase cloud formation. *J. Geophys. Res. Atmos.* **2012**, *117*(D16209). DOI: 10.1029/2012jd018063.